Late Miocene K-rich volcanism in the Eslamieh Peninsula (Saray), NW Iran: Implications for geodynamic evolution of the Turkish–Iranian High Plateau

H. Shafaii Moghadam [a,1], G. Ghorbani [a], M. Zaki Khedr [b,c], N. Fazlnia [d], M. Chiaradia [e], Y. Eyuboglu [f], M. Santosh [g], C. Galindo Francisco [h], M. Lopez Martinez [i], A. Gourgaud [j], S. Arai [b]

[a] School of Earth Sciences, Damghan University, Damghan 36716-41167, Iran
[b] Department of Earth Sciences, Kanazawa University, Kanazawa 920-1192, Japan
[c] Department of Geology, Faculty of Science, Kafrelsheikh University, Egypt
[d] Department of Geology, Urumieh University, Urumieh, Iran
[e] Département de Minéralogie, Université de Genève, Genève, Switzerland
[f] Department of Geological Engineering, Karadeniz Technical University, 1080 Trabzon, Turkey
[g] School of Earth Sciences and Resources, China University of Geosciences, 29 Xueyuan Road, Beijing 100083, China
[h] Departamento de Petrología y Geoquímica, Universidad Complutense- IGEO (UCM-CSIC), 28040 Madrid, Spain
[i] Departamento de Geología, Centro de Investigación Científica y de Educación Superior de Ensenada (CICESE), Carretera Ensenada–Tijuana No. 3918, 22860 Ensenada, Baja California, México [j] UMR 6524 "Magmas et volcans", OPGC–Université Blaise Pascal–CNRS, 63038 Clermont-Ferrand Cedex, France

A B S T R A C T

Post-collisional volcanism in northwestern Iran is represented by the Saray high-K rocks including leucite-bearing under-saturated and leucite-free silica saturated rocks. We report Ar–Ar age data which constrain the age as ca. 11Ma (late Miocene). Most of clinopyroxene phenocrysts from the volcanic rocks have complex oscillatory zoning, with high Ti and Al cores, low Ti and high Al mantled clinopyroxenes, grading into low Ti and Al outer rims. All the rocks are highly enriched in incompatible trace elements and have identical Sr–Nd–Pb isotopes. Enrichment in incompatible elements and other geochemical features for the Saray lavas suggest a metasomatized sub-continental lithospheric mantle (SCLM) as the magma source. The negative Nb–Ta–Ti anomalies for the Saray lavas compare with the features of subduction-related magmatism with negligible contamination with ancient crustal components. The highly radiogenic $^{87}Sr/^{86}Sr$ and $^{207}Pb/^{204}Pb$ isotopic values of the Saray lavas imply the involvement of slab terrigenous sediments and/or a continental lithosphere. Isotopically, the volcanic rocks define a binary trend, representing 5–8% mixing between the primary mantle and sediment melts. Our melting models suggest residual garnet in the source and are incompatible with partial melting of amphibole and/or phlogopite bearing lherzolites, although the complex geochemical features might indicate the result of mixing between melts produced by different sources or a homogenous melt passing through a compositionally-zoned mantle during multiple stages of partial melting and melt migration. The geochronological, geochemical and isotopic data for the Saray rocks suggest that these Late Miocene magmas were derived from a small degree of partial melting of subduction-metasomatized (subcontinental) lithospheric mantle source in a post-collisional setting.

Keywords: High-K lavas Geochemistry, Sr–Nd–Pb isotopes, Post-collisional magmatism Iran

1. Introduction

The northward migration of the Afro-Arabian plate caused subduction during the late Cretaceous to Miocene beneath the Iranian block, followed by collision between the Anatolian–Iranian and Arabian plates during middle to late Miocene (Berberian and King, 1981; Alici Sen et al., 2004; Chiu et al., 2013). This continental collision was accommodated by crustal shortening and thickening in eastern Anatolia and northwestern Iran (Sengor and Yılmaz, 1981; Temel et al., 1998; Alici Sen et al., 2004; Dilek et al., 2010). The northwestern Iran–eastern Mediterranean region (Turkish–Iranian High Plateau) is a tectonically active plateau between the converging Arabia and Eurasia. Cenozoic magmatic rocks occur extensively in the Turkish–Iranian High Plateau, northeast of the Bitlis–Zagros suture zone (Dilek et al., 2010) (Fig. 1). The temporal distribution of the magmatism in this region shows different phases of magma generation with distinct geochemical signatures mainly in the late Eocene, late Miocene and Plio–Quaternary (Dilek et al., 2010; Eyuboglu et al., 2010, 2011a,b,c,d,e, 2012, 2013a,b). Mantle-derived volcanic rocks with oceanic-island basalt (OIB)-like geochemical features with and/or without subduction fingerprints are commonly found in the Turkish–Iranian High Plateau (e.g., Aldanmaz et al., 2006; Dilek and Altunkaynak, 2009; Kheirkhah et al., 2009; Elitok et al., 2010; Allen et al., 2013).

E-mail address: hadishafaii@du.ac.ir (H.S. Moghadam).
[1] Tel.: +98 9132762361.

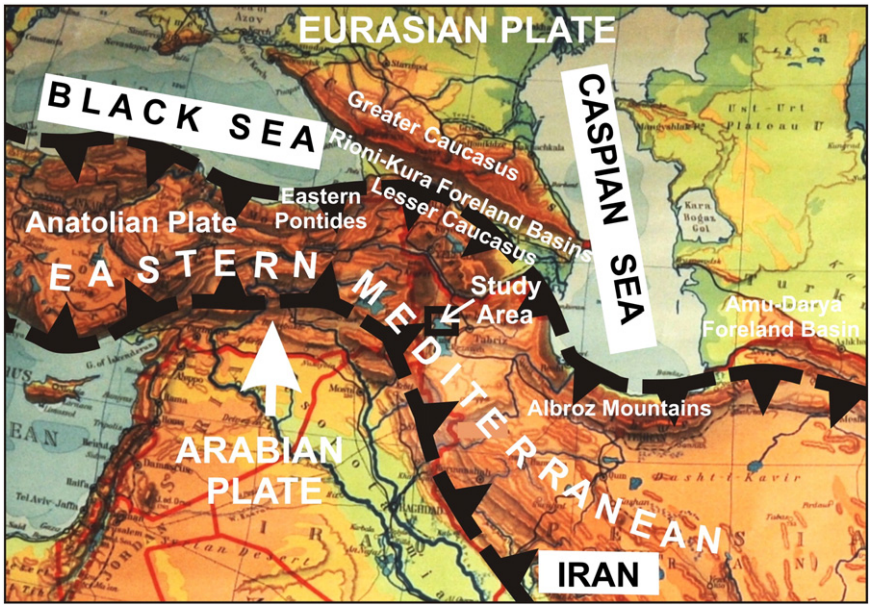

Fig. 1. Simplified tectonic map of the eastern Mediterranean–Persian Gulf region, showing the active plate boundaries and location of the eastern Pontides–Lesser Caucasus–Albroz magmatic arc.
Modified after Eyuboglu et al. (2012).

The late Miocene magmatic rocks with calc-alkaline and shoshonitic (or ultrapotassic) characteristics are found mainly along the UDMA (Chiu et al., 2013) and occur in the northern parts of the Turkish–Iranian High Plateau (Moine-Vaziri et al., 1991; Dilek et al., 2010; Eyuboglu et al., 2012). Plio-Quaternary magmatic rocks are represented by alkaline rocks with and/or without subduction overprints and by shoshonitic rocks in several regions of the UDMA, but mostly in NW Iran, in the Turkish–Iranian High Plateau (e.g., Keskin, 2003; Kheirkhah et al., 2009; Elitok et al., 2010; Eyuboglu et al., 2012; Allen et al., 2013).

The study area is situated between the Bitlis–Zagros Zone and eastern Pontides–Lesser Caucasus–Albroz magmatic arc. Although there is consensus on a northward subduction model for the geodynamic evolution of the Bitlis–Zagros Zone in the southern part of the study area, the evolution of the eastern Pontides–Lesser Caucasus–Albroz magmatic arc in the north is still controversial due to lack of systematic geological, geochronological and geochemical data. The most popular idea is the magmatic arc developed by the northward subduction of the Paleotethys oceanic lithosphere, which was situated to the south of the arc, until the Eocene (e.g., Adamia et al., 1977; Okay and Sahintürk, 1997; Dilek et al., 2010). An earlier interpretation by Sengor and Yılmaz (1981) proposed that Paleotethys was located to the north of the magmatic arc, and hence southward subduction operated from the Paleozoic until the Dogger, and that northward subduction occurred subsequently from the late Mesozoic until the Eocene. The third model includes those of Dewey et al. (1973), Bektaş et al. (1999), Chorowicz et al. (1998), Eyuboglu et al. (2006, 2007, 2010) and Eyuboglu (2010) who favor a southward subduction of the Tethys oceanic lithosphere, which was situated to the north of magmatic arc, continued uninterruptedly from the Paleozoic till the late Cenozoic.

Adakitic volcanism is minor in the region north of the Bitlis–Zagros suture zone in the northern and southern parts (e.g., Jahangiri, 2007; Omrani et al., 2008; Chiu et al., 2013). However, different pulses of magmatism are widespread in the Eastern Pontides–Lesser Caucasus and eastern Iranian–Azerbaijan regions, which have been correlated with the northward subduction of the southern Neotethyan Ocean (Yılmaz et al., 1997). These rocks vary in composition from calc-alkaline to alkaline/adakitic characteristics with temporal variations from Paleocene to Plio-Quaternary. The occurrence of magmatic rocks in the Eastern Pontides–Lesser Caucasus and eastern Iranian–Azerbaijan regions have posed important questions related to the geodynamic evolution of these regions. Recent comprehensive geological, geochemical, and geochronological studies (e.g., Dokuz, 2011; Eyuboglu et al., 2011a,b,c,d,e, 2012, 2013a, 2013b; Maden, 2013) on the Cenozoic magmatism revealed that the adakitic magmatism occurred in two different cycles in the eastern Pontides–Lesser Caucasus–Alborz magmatic arc. The first phase was during the late Paleocene–early Eocene and the second one during late Miocene. The origin of the late Paleocene–early Eocene adakitic rocks, which are well exposed in the southern part of the eastern Pontides orogenic belt, has been correlated to slab window processes in a southward subduction zone (Eyuboglu et al., 2011a,b,c,e, 2013a,b). The late Miocene adakitic rocks, which are well exposed in the eastern part of the eastern Pontides orogenic belt and also Caucasus, were generated by partial melting of the mafic lower crust after the collision between Lesser Caucasus and Greater Caucasus (Eyuboglu et al., 2012). These studies suggest that the slab break-off of the southward subducted oceanic lithosphere and inflow of hot asthenosphere into the mantle wedge caused partial melting of subduction-modified mantle wedge and led to the formation of Pliocene and Pleistocene alkaline magmatic rocks exposed along the northern edge of the eastern Pontides–Lesser Caucasus–Albroz magmatic arc (Eyuboglu et al., 2012). Although several studies have highlighted the temporal and spatial aspects of magmatism in the Turkish–Iranian High Plateau, showing different pulses of magma generation mainly in the late Eocene, late Miocene and Plio–Quaternary and with distinct geochemical signatures, NW Iran has not been investigated in detail. A recent report shows that Late Eocene and Oligocene (ca. 38 to 23 Ma) shoshonitic to adakitic plutons (with an age progression from SE to NW) are common in NW–N Iran (Castro et al., 2013). It is important to trace the temporal distribution of the various pulses of magmatism and the triggering mechanisms in NW Iran, in order to evaluate the post-collisional magmatism in this region.

In this paper we present: 1) a detailed classification of the high-K volcanic rocks in the Eslamieh Peninsula (Saray) based on mineral and whole rock geochemical studies; 2) Ar–Ar dating of the rocks and 3) Sr–Nd–Pb isotope geochemistry. Based on the results, we evaluate the petrogenesis of the high-K rocks (leucite-free or leucite-bearing) and its implications on post-collisional magmatism in the late Miocene.

We then interpret our data in the geodynamic framework of the Turkish–Iranian High Plateau in order to constrain the mantle source and magma evolution of high-K volcanic rocks.

2. Geological setting and field relationships of high-K volcanic rocks

The late Miocene (Tortonian) high K-volcanic rocks are exposed mainly in the Eslamieh Peninsula (Saray), to the southeast of Urumieh city (Figs. 1 and 2). The contact relationships with older strata, including the magmatic and metamorphic basement (such as the Gushchi A-type granites and Cadomian granitic gneisses), are mostly covered by younger salty-clay deposits of the Urumieh Lake. The late Miocene high-K Saray volcanic rocks appear to crosscut the Iranian basement. The Cadomian granitic gneisses show similarity to those described in central Iran by Hassanzadeh et al. (2008). The Gushchi A-type granites are associated with OIB-

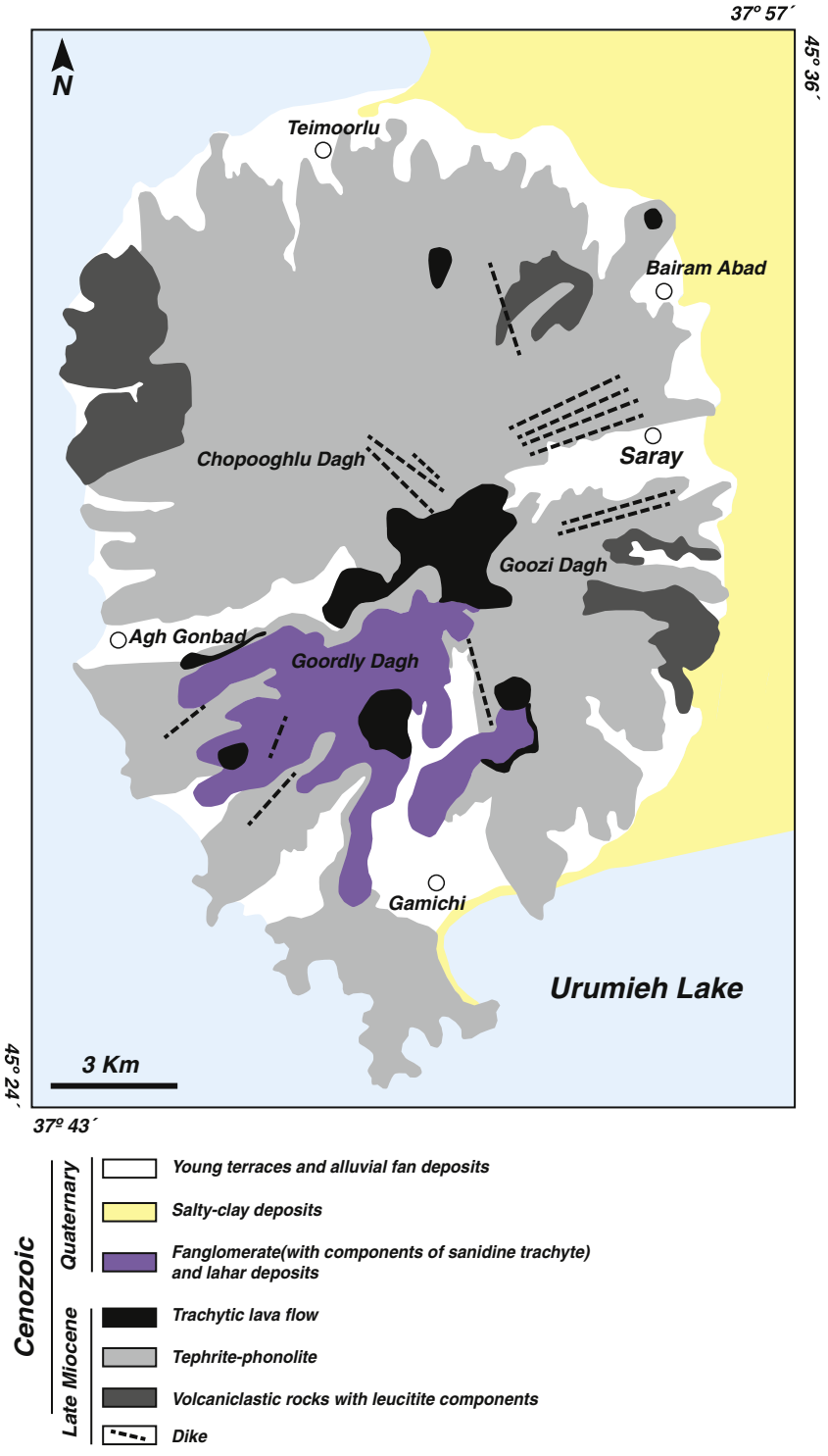

Fig. 2. Simplified geological map of the Eslamieh (Saray) Peninsula. Modified after Moine-Vaziri et al. (1991).

type alkaline gabbros and show intrusive contacts with these alkaline rocks. The gabbroic rocks yielded Ar–Ar ages of ca. 316 Ma, although they seem to be older than 360 Ma, indicating a phase of Ar resetting (Shahabi, 2013).

Field observations show that the volcanic activity in the Saray can be divided into six major stages as follows. (i) An older, probably early Miocene (Aquitanian–Langhian) plutonism represented by nepheline–syenite and monzonite xenoliths within the high-K volcanic rocks.(ii) Late Miocene (Tortonian) explosive activity initiated with a major caldera-forming episode. This magmatic episode is composed of basanite, leucite–tephrite and pyroclastic rocks in the lower volcanic unit and phonolite, trachyte and analcime-bearing basanite in the upper volcanic unit (Moine-Vaziri et al., 1991). (iii) A phase of highly explosive activity with deposition of a thick pyroclastic sequence. The rock fragments in these pyroclastic assemblages are similar to the volcanic rocks of stage (ii) or are petrographically (see Section 3) different. Clinopyroxene–phlogopite–feldspar-rich cumulate-like (autholite) xenoliths are rare in the pyroclastic rocks and might indicate that the crystals accumulated in crustal magma chambers. The rock fragments vary in size between 4–5 cm to even N1 m. (iv) Trachytic and leucite–clinopyroxene tephritic dikes are injected in the previously emplaced volcanic (stage ii) and/or in pyroclastic units (stage iii). The dikes are variable in size, from 30–40 cm up to 2m. Near the Saray village, a set of dikes with different composition are injected within the pyroclastic rocks. Rarely, the earlier dikes crosscut the older ones. (v) A late stage phase mainly accompanying the Lahar formation. (vi) Caldera collapse stage and formation of ring and radial lamprophyric dikes, cutting the lahar deposits near the Saray village. Lamprophyric sills and tephritic–basanitic dikes are found elsewhere within the lahar deposits, far from the Saray caldera. Moreover, clinopyroxene-rich tephritic lavas occur within the lahar deposits, in the absence of any sharp contacts, and with a red-colored paleosol.

Magmatic activity of stage ii is mainly characterized by at least five successive cycles. The first cycle is characterized by a pyroclastic sequence with leucite or analcimized leucite-bearing tephritic and/or leucititic (40–80% leucite) rock fragments. Trachytic lavas with large sanidine phenocryts represent the second cycle followed by leucite–clinopyroxene-rich tephrites (third cycle). The fourth cycle is a combination of thick (70–80 m) leucite-bearing tephritic lavas and subsequent pyroclastic breccias. Dikes (even 30 m thick) are common within the leucite tephrites. Highly vesicular, leucite-bearing tephritic lavas rest over the pyroclastic rocks (fifth cycle). The contact of the rocks shows peperitic characteristic with red-colored bombs and pumiceous lavas.

3. Petrography of high-K volcanic rocks

About 60 thin sections from all rock units of the Saray potassium-rich rocks were examined in this study. From these, nine representative samples were selected for microprobe analyses, thirty samples for whole rock major and trace (REE) element analyses, two samples for Ar–Ar dating and 8 samples for Sr–Nd–Pb isotope studies (see Appendix 1 for analytical methods).

Nomenclature and classification of high-K rocks have been long debated (e.g., Foley et al., 1987; Mitchell and Bergman, 1991). The complex mineralogy of these rocks is attributed to the complex chemical compositions of their source magma(s) (e.g., Foley et al., 1987; Conticelli et al., 2012) and subsequent mixing between two types of magmas and/or assimilation of crustal materials. Here we adopted a classification based on field occurrence, petrographic features and mineral modes. Thus, we subdivided the rocks into seven groups including trachytic–phonolitic–tephritic lavas, tra-chytic dikes in pyroclastic sequences, rock fragments in volcaniclastic rocks, tephritic–basanitic dikes, leucititic lavas, lamprophyric dikes within lahar deposits and nepheline syenite xenoliths.

3.1. Trachytic–phonolitic–tephritic lavas (nepheline-bearing)

The trachytic lavas consist mainly of highly zoned, euhedral to rarely subhedral and green clinopyroxene phenocrysts (0.5–1 mm). Phlogopite (biotite) is surrounded by fine-grained Fe-oxide grains, which can be correlated to the breakdown of phlogopite during decompression and the oxidizing conditions during eruption. Fine-grained (0.2–0.3 mm) microphenocrysts of nepheline occur rarely. Apatite and zircon occur as tiny inclusions within pyroxene. The groundmass is composed of sanidine and plagioclase (with anorthoclase) associated with clino-pyroxene and phlogopite microlites (Fig. 3B). Oxide minerals are common within the groundmass. Greenish sodic amphiboles occur around the clinopyroxene grains. Leucite and analcimized leucite (>0.5 mm but av. = 0.2–0.3 mm) associated with apatite and clinopyroxene with a potassium feldspathic groundmass is widespread in the phonolitic–tephritic lavas (Fig. 3A and F). Euhedral to subhedral, olivine phenocrysts (<0.5 mm but rarely 2 mm) are abundant in basanites. Ocelli texture is common in the fine-grained groundmass of some basanites. Two types of clinopyroxenes are common within the tephrites; 1 — green and sodic clinopyroxene, subhedral to euhedral with sieve texture (0.5–1 mm) and 2 — large (>1 mm) clinopyroxene with pale-green or colorless core and green rim. The interstices in the tephritic lavas are filled by perthitic alkali feldspar.

3.2. Trachytic dikes in pyroclastic units

These rocks are porphyritic, with clinopyroxene and phlogopite microphenocrysts. Sanidine microlites, oxide minerals and fine-grained clinopyroxene and phlogopite crystals are abundant in the groundmass. Trachytic dikes have two types of clinopyroxrenes; pale-green and deep green varieties (Fig. 3E). Titanite is common in some of these dikes.

3.3. Rock fragments in volcaniclastic rocks

The rock fragments within volcanic breccias show different modal compositions and can be subdivided into quartz monzonite to quartz monzo-syenite fragments, nepheline-bearing monzonites, tephrites and tephritic tuffs. Euhedral to subhedral plagioclase phenocrysts (1–2 mm) with alteration into clay and sericite are abundant in the quartz-monzonite to quartz monzo-syenitic rock fragments. Anhedral and fine-grained quartz crystals (<20 vol.%) are present between plagioclase laths and accompany the K-feldspar grains. K-feldspar occurs as interstitial phase between other minerals. Deep-green clinopyroxene and apatite microphenocrysts make the other rock components. Nepheline (<2 vol.%) associated with sodic clinopyroxenes, plagioclase, K-feldspar, phlogopite and amphibole occur in nepheline bearing monzonites and/or monzo-syenites. The tephritic tuffs contain lithic fragments and altered glass shards. Olivine, green and/or colorless clinopyroxenes and K-feldspar crystal fragments are abundant.

3.4. Tephritic-basanitic dikes in volcanic and/or pyroclastic rocks

Zoned large (3–4 mm) and medium (1 mm) clinopyroxene grains are the major components in these rocks. The core of some large-sized clinopyroxenes exhibits a pale-green color while their rim shows a deep green color. The clinopyroxenes locally exhibit sieve-textured domains surrounding the clear core (Figs. 3D and 4c). The evolution of the sieve texture is widely attributed to changes in temperature, pressure and composition in the magma (e.g., Tsuchiyama, 1985; Nelson and Montana, 1992). Euhedral to subhedral olivine (1 mm to <1 mm) is common, showing slight alteration into iddingsite (Fig. 3D). Large to small grains of leucite phenocrysts (or analcimized leucite) (<1 mm) are abundant (Fig. 3C). Alkali-feldspar overgrowth around the leucite is also noticed. Nepheline microphenocrysts are rare. The groundmass of these rocks is holocrystalline, composed of K-feldspar, clinopyroxene, oxide minerals and fine-grained, highly altered olivine

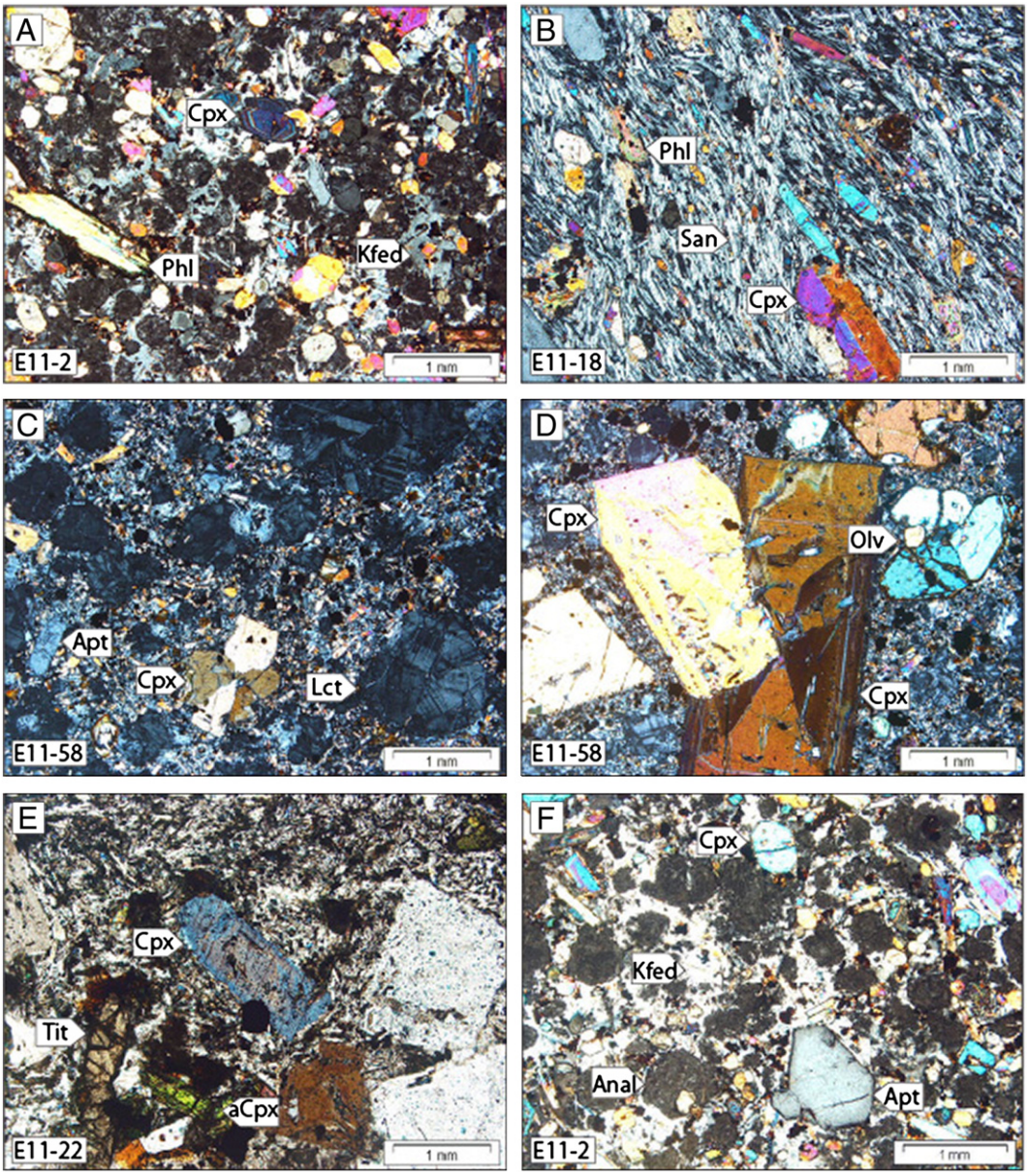

Fig. 3. Photomicrographs of the Saray high-K rocks. (A) Phlogopite and clinopyroxene microphenocrysts in a groundmass composed of alkali-feldspar in phonolitic lavas; (B) Sanidine microlites defining trachytic texture associated with phlogopite and clinopyroxene in trachytic lavas; (C) Leucite phenocrysts and apatite–clinopyroxene microphenocrysts set in a fine-grained groundmass in basanitic dikes; (D) Olivine and euhedral, zoned clinopyroxene phenocrysts in basanitic dikes; (E) Titanite, deep green, high Ti–Al clinopyroxene (aCpx) and pale green, low Ti–Al clinopyroxene (Cpx) in trachytic dikes; (F) Analcimized leucite (Anal), clinopyroxene and apatite microphenocrysts in a groundmass containing K-feldspar in phonolitic lavas.

crystals. There are two generations of clinopyroxene in most of the dikes; 1 — colorless clinopyroxenes, sometimes with a pale green, thin rim; 2 — green clinopyroxene. The occurrence of these two clinopyroxene types might indicate mixing between alkaline and crustal-derived magmas. Most of the pyroxenes exhibit sieve texture, again suggesting a magma mixing process, although this feature could also reflect rapid decompression and volatile loss in a magma that has not been mixed.

3.5. Leucitite lavas

These rocks are represented by the occurrence of subhedral to euhedral, large leucite phenocrysts (av. = 0.5 mm up to >4 mm) and large (av. = 0.5–1 mm up to >5 mm) zoned sodic clinopyroxenes. Leucite constitutes >60 vol.% of these rocks. Olivine, apatite (0.2–0.3 mm) and oxide minerals (<0.1 mm) microphenocrysts are common. Some clinopyroxenes exhibit resorbed texture. Leucites have clinopyroxene inclusions. The groundmass of the rocks is holocrystalline with clinopyroxene and leucite fine-grained crystals.

3.6. Nepheline syenite xenoliths

Xenoliths contain very large (>6 mm but mostly 2–4 mm) nepheline phenocrysts. Deep-green, sodic clinopyroxenes, phlogopite and albite are present between the nepheline crystals (Fig. 4D). Biotite and clinopyroxene are elongated prismatic in shape with width/length ratio of around 1/7 to 1/20 for biotite and 1/5 to 1/10 for clinopyroxene. Brown amphiboles are present around the clinopyroxene. Sphene occurs as euhedral and primary (magmatic) crystals. Apatite, clinopyroxene and phlogopite are included within nepheline crystals.

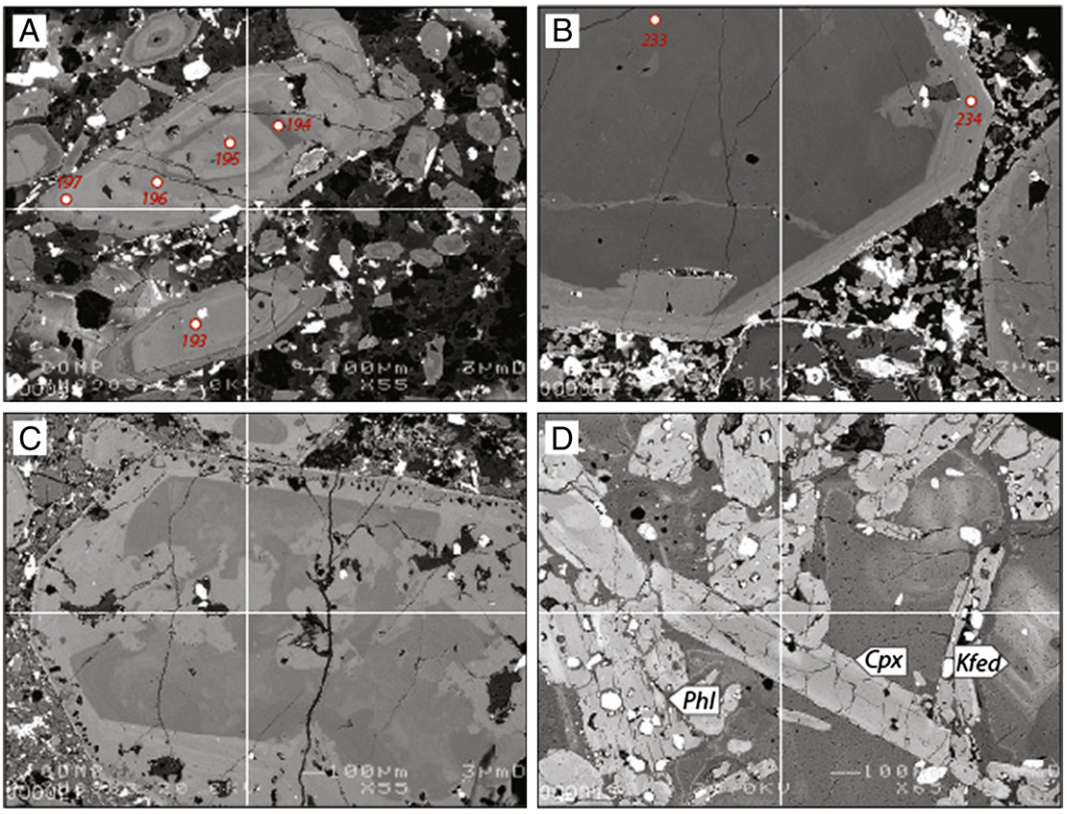

Fig. 4. Back-scattered electron images of the Saray high-K rocks. Numbers denote the locations of EMPA analysis from the complexed zoned grains in terms of Al_2O_3 and TiO_2. (A) Sample E11-2, phonolitic lava (point 193, TiO_2 =0.37wt.%, Al_2O_3 =1.7 wt.%; point 194, TiO_2=0.57, Al_2O_3=2.9; point 195, TiO_2 =1.2, Al_2O_3=2.4; point 196, TiO_2 =0.6, Al_2O_3=2.9; point 197, TiO_2=0.37, Al_2O_3=1.9); (B) Sample E11-58, basanitic dike (point 233, TiO_2=0.32, Al_2O_3=1.7; point 234, TiO_2=1.3, Al_2O_3=5.3); (C) Resorption texture with irregular outlines in relict clinopyroxene (poor in Al and Ti, deep gray) mantled by new clinopyroxene (rich in Al and Ti, light gray) in sample E11-17 (phonolitic lava). The rim of clinopyroxene grain exhibits sieve texture; (D) Phlogopite, green-colored clinopyroxenes and alkali feldspar in syenitic xenoliths.

3.7. Lamprophyric (sannaite) dikes within lahar deposits

Olivine, clinopyroxene and phlogopite are the main constituents of the lamprophyric dikes, set in a groundmass composed of altered alkali-feldspar and sodic clinopyroxene microlites. Clinopyroxenes are either pale-green and zoned (0.5–1 mm) or colorless (0.2–0.3 mm).

4. Mineral, whole rock and Sr–Nd–Pb isotopes geochemistry

4.1. Mineral chemistry

4.1.1. Clinopyroxene

Following the classification of Morimoto et al. (1998), all clinopyroxenes of the K-rich rocks including the tephritic rocks frag-ments in volcaniclastic rocks, phonolitic–trachytic lavas, basanitic dikes, trachytic as well as sannaitic dikes are dio psid e (Fig. 5A) with variable X_{Mg} values (molar Mg/Mg + Fe^{2+}) of 0.61–0.93. The Al and Ti contents of clinopyroxenes are highly variable, ranging from 0.05 to 0.37 and b0.01 to 0.06 a.f.u. (Appendix 2a). In the clinopyroxenes from trachytic–phonolitic–tephritic (TPT) lavas, Al is not sufficient to fill completely the tetrahedral site, similar to clinopyroxenes fromMediterranean lamproites (e.g., Cellai et al., 1994; Conticelli et al., 2012) (Fig. 5B). Most of the clinopyroxenes from tephrtic–basanitic dikes have higher Al and Ti contents similar to transitional high-K rocks of Conticelli et al. (1997)(Fig. 5B).

Clinopyroxene phenocrysts of the Saray volcanic rocks display oscillatory zoning, with high Ti and Al cores, mantled by low Ti and high Al clinopyroxenes, and grading into low Ti and Al outer rims, and/or vice versa, with poor Al–Ti core rimmed by high Ti–Al clino-pyroxenes (Fig. 4A,B). The older clinopyroxenes typically show complex resorbed grain margins with a rim of high Ti–Al clinopyroxene (Fig. 4C). The rim shows a sieve texture, denoting decompression during the rapid ascent of the magma to the surface. The Cr content of the clinopyroxenes is relatively low (Cr_2O_3 b 0.5 wt.%) (Appendix 2a).

4.1.2. Feldspar

Plagioclase is rare in the high-K rocks, except as a minor component in the tephritic rock fragments and shows labradorite composition (An_{53}) (Fig. 5C). Potassium feldspar microlites of the Saray volcanic have a fairly large compositional range between Or_{15} and Or_{98}. The alkali feldspars in tephritic rock fragments have anorthoclase com-position ($An_{11-19}Ab_{60-97}Or_{15-29}$) (Appendix 2d). The Fe content of feldspar grains varies between 0.12 and 0.86 wt.% (Appendix 2d).

4.1.3. Mica

The mica in the Saray volcanic rocks has biotite to phlogopite composition with X_{Mg} ranging from 0.58 to 0.89. Their Al_2O_3 is nearly constant with limited variation between 11.3 and 13.5 wt.%. These micas plot in the alkaline and calc-alkaline lamprophyric fields of Rock's (1987) diagram (Fig. 6A). The TiO_2 and Cr_2O_3 abundances of the Saray micas vary from 1.4 to 8.2 and 0 to 0.6 wt.% respectively. The mica composition seems to be different in various types of the Saray lavas including high Ti but low Fe and high Fe and low Ti varieties (Appendix 2b). Some of the micas are high Ti phlogopites, and the charge balance with Ti^{4+} might require a tetraferriphlogopite component — i.e., Fe^{3+} in the tetrahedral site.

4.1.4. Opaque minerals

Opaque minerals in the Saray volcanic rocks are generally re-presented by magnetite and Ti–magnetite (Fig. 6B). These grains are

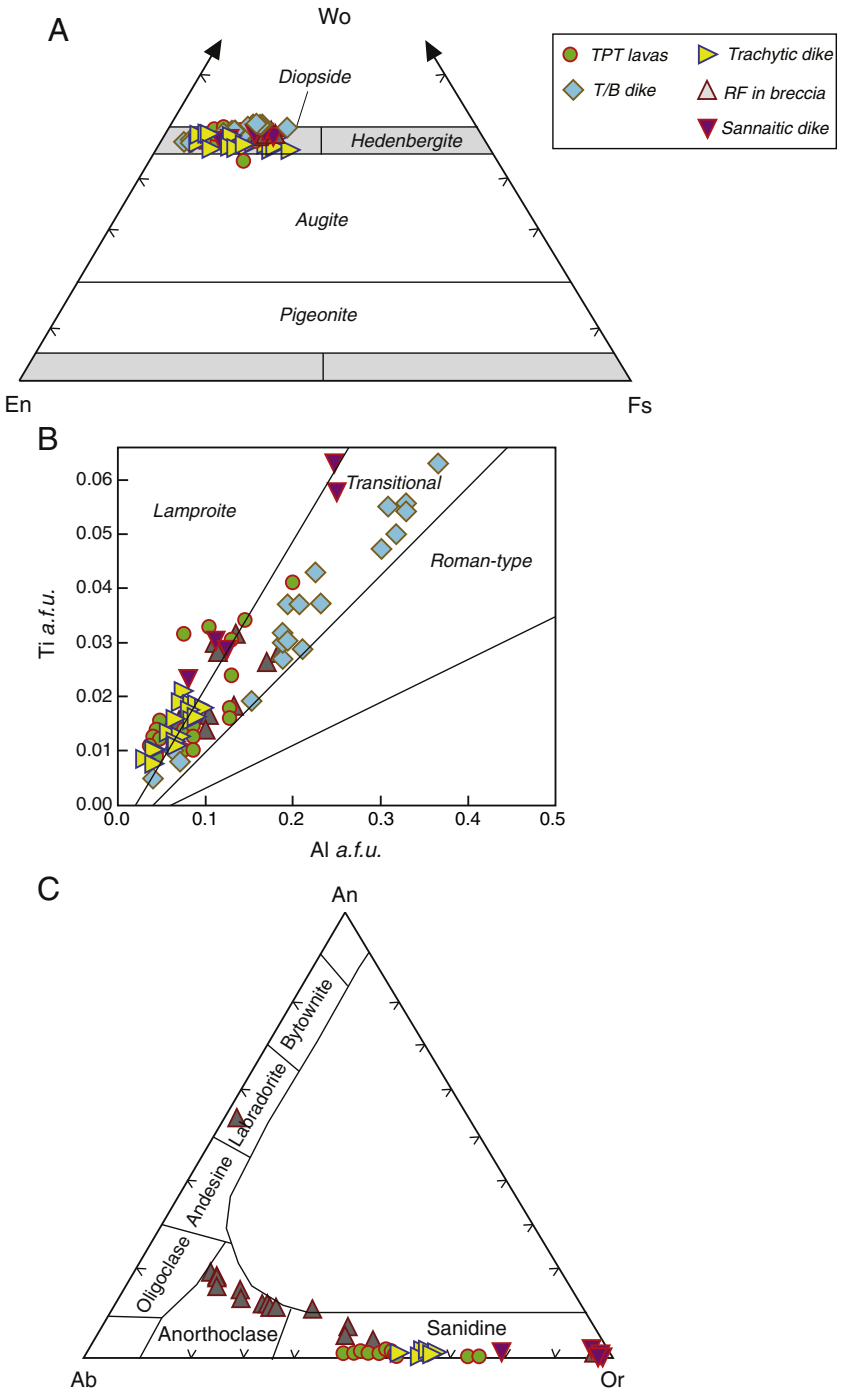

Fig. 5. (A) Compositional variety of clinopyroxene in high-K rocks in wollastonite (Wo)–enstatite (En)–ferrosilite (Fs) diagram; (B) Ti vs. total Al, expressed as atoms per formula unit (a.f.u.) in clinopyroxenes of high-K rocks; (C) Composition of feldspar expressed in the orthoclase (Or)–albite (Ab)–anorthite (An) diagram.
Modified after Conticelli et al. (2012).

characterized by highly variable contents of MgO (0.04–7.8 wt.%) and TiO_2 (0.36–23.61 wt.%) (Appendix 2c).

4.1.5. Leucite and analcimized leucite

Leucite phenocrysts are characterized by high contents of K_2O (20–22wt.%) and Al_2O_3 (22–24 wt.%) whereas the analcimized leucites have lower K_2O (9 –14 wt.%) and Al_2O_3 (19–23 wt.%) (Appendix 2d, f), but with higher water content. Na_2O abundance of leucite and analcimized leucite varies from 0.02 to 0.4 and 0.1 to 3.8 wt.%respectively.

4.1.6. Apatite

Apatite occurs as microphenocrysts in the Saray high-K rocks with low levels of FeO (0.1–0.8 wt.%) (Appendix 2g).

4.1.7. Olivine

Olivine in the Saray high-K rocks varies in composition from Fo_{76} to Fo_{91}, mostly from the core of polygonal to resorbed crystals. NiO shows positive correlation with forsterite content whereas CaO shows a negative correlation (Fig. 6C,D), with NiO reaching values as high as 0.2 wt.% (Appendix 2h), different from those of the lamproitic rocks. Olivine displays a decrease of CaO with increasing forsterite, in contrast

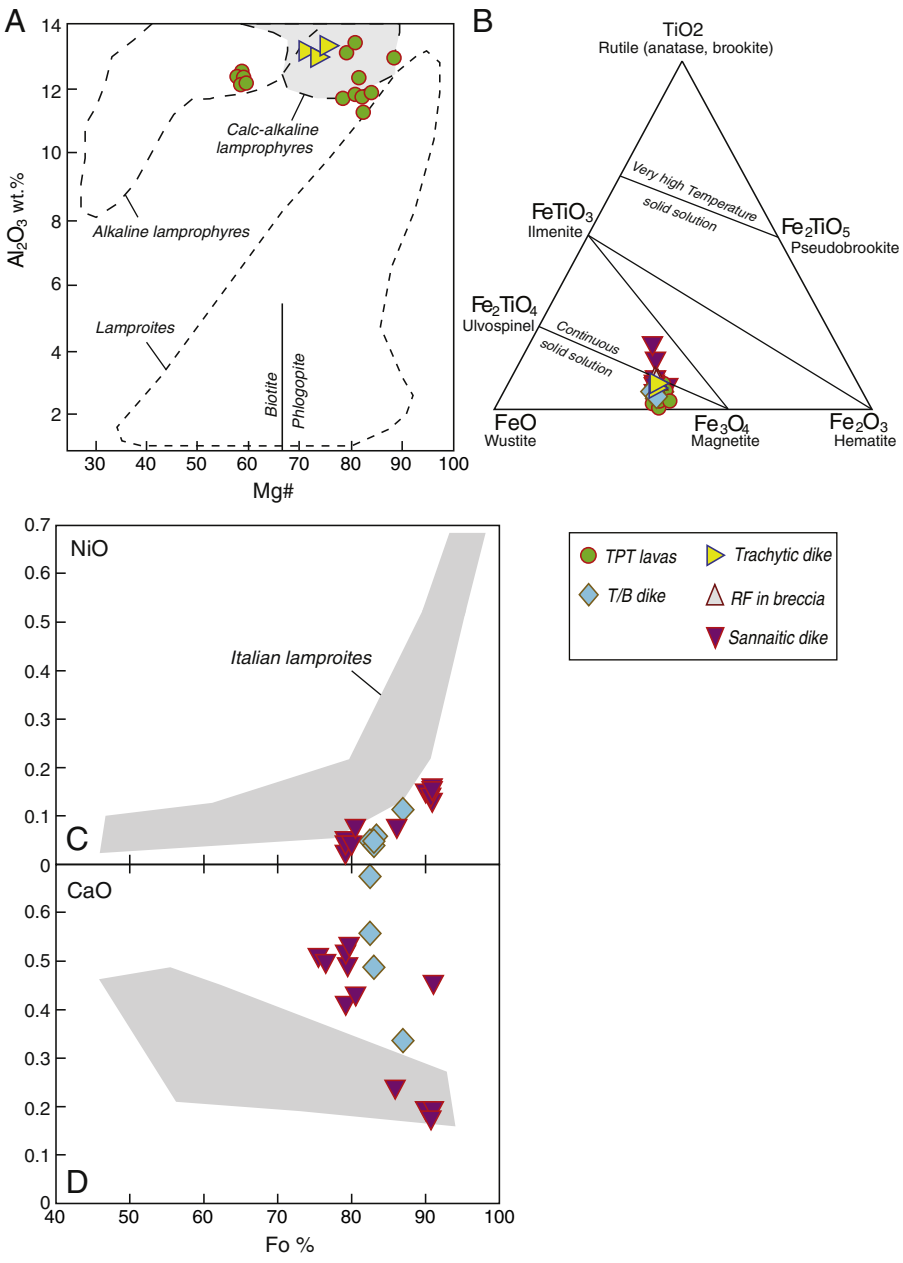

Fig. 6. Compositional plots for discriminating mica (A), opaque minerals (B) and olivine (C and D) compositions in the Saray high-K rocks. a was modified after Rock (1987); b, after Buddington and Lindsley (1964); and c, after Conticelli et al. (1992), Prelević and Foley (2007), and Conticelli et al. (2012).

to the trend suggested for lamproitic rocks by Conticelli and Peccerillo (1992), Conticelli et al. (2012) and Prelević and Foley (2007).

4.1.8. Nepheline

Nephelines in these rocks have high contents of Na_2O (15.4–16.3 wt.%), Al_2O_3 (29.7–31.2 wt.%) and low contents of K_2O (2.8–3 wt.%) (Appendix 2j).

4.2. Whole rock geochemistry

Major and trace (REE) element analyses of representative high-K samples are listed in Appendix 3. The LOI of the Saray high-K rocks vary between 0.2 and 6.1 wt.% but most of them (22 samples) have less than 2 wt.% LOI. High LOI values are common in the samples with analcimized leucites and altered glass groundmass. Owing to the relatively high LOI values of some samples, all major elements have been recalculated to 100% on the water-free basis for plots in variation diagrams.

The Saray volcanic rocks (and nepheline syenite xenoliths) were classified using the total alkalis ($K_2O + Na_2O$ wt.%) vs. SiO_2 diagram of Le Bas et al. (1986) (Fig. 7A). The high-K rocks fall in a wide range represented by tephrite to phonolite/trachyte and trachy-andesite fields, in accordance with their petrographic features. All Saray volcanic rocks lie within shoshonite to ultrapotassic fields defined by Peccerillo and Taylor (1976) (Fig. 7B). These volcanic rocks display a low to high potassic affinity (K_2O N Na_2O) with K_2O/Na_2O ratios ranging from 0.6 to 4.5 (Appendix 3).

In the CaO vs. Al_2O_3 and MgO diagrams of Foley et al. (1987), most of the Saray high-K rocks display affinity to Roman-type ultrapotassic rocks (Fig. 7C,D). These rocks are different from normal lamproites

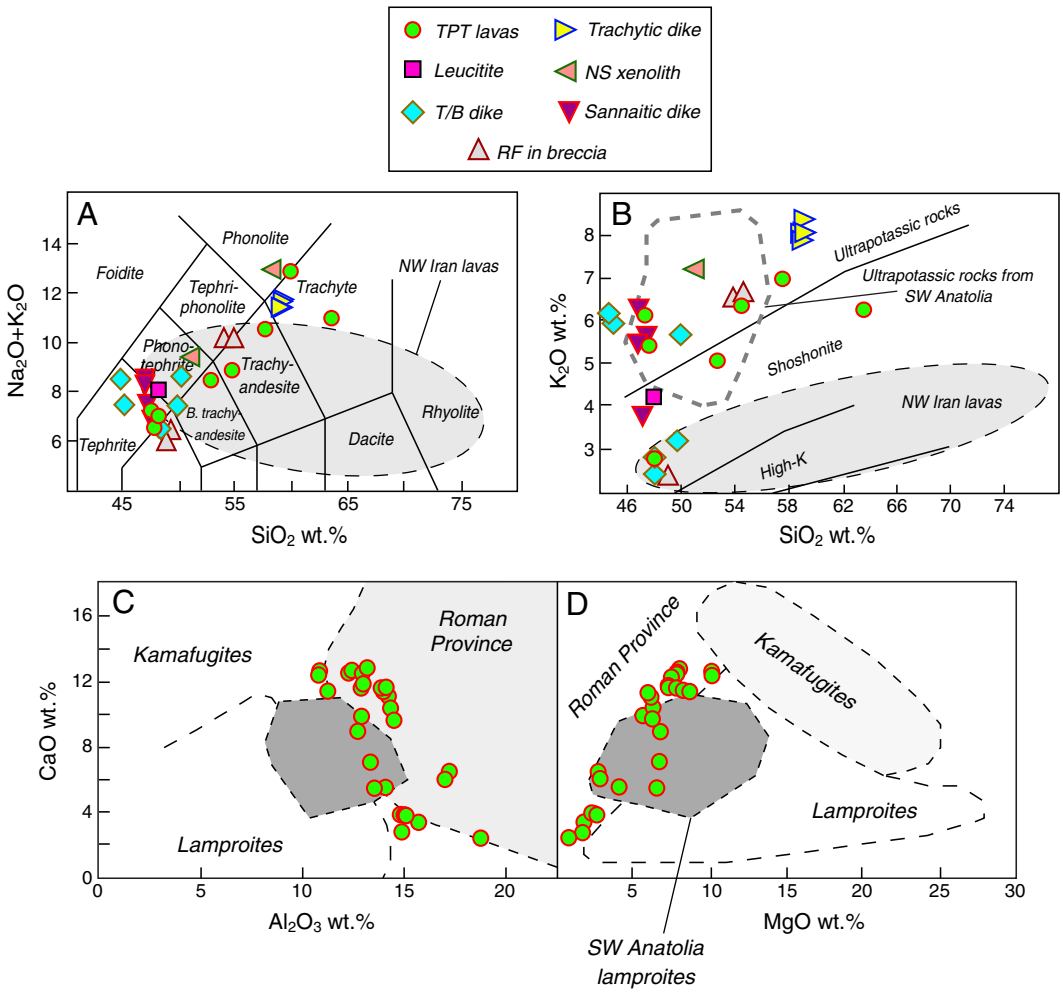

Fig. 7. (A) Total alkalis vs. SiO_2 diagram for the high-K volcanic rocks of Saray. All the major elements data have been recalculated to 100% anhydrous basis; (B) K_2O vs. SiO_2 classification diagram of the Saray volcanic rocks; (C and D) The Turkish high-Mg mantle-derived ultrapotassic rocks of lamproitic affinity in the classification diagrams of Foley et al. (1987).
a w a s m o d i fied after Le Bas et al. (1986).

(group 1 lamproites; e.g., Foley et al., 1987; Prelević et al., 2008) b y having higher CaO and Al_2O_3, a n d l o w e r K_2O/Al_2O_3 ratios and markedly low MgO content. Some high-K lavas possess a lamproitic signature, resembling the SW Anatolian lamproites and/or Mediterranean lamproites in their higher Al_2O_3 and lower MgO contents. The Saray high-K rocks display negative trends between SiO_2 and CaO, TiO_2, C a O , FeO and relatively positive correlation with Al_2O_3. Although K_2O a n d Na_2O show scatter, they display an increasing trend with SiO_2 (Fig. 8). The variations observed above could reveal fractional crystallization processes. Although the complex history of zoning in minerals, especially clinopyroxene, is similar to the cases of magma mixing, fractional crystallization of a mixed magma (and/or mixing between differently fractionated magmas) is indicated by the Harker-type diagrams. For example, the decrease in CaO might be related to the fractionation of clinopyroxene, FeO^t and TiO_2 to Fe–Ti oxides plus olivine. High CaO content in most of the samples reflect clinopyroxene accumulation, as also testified by petrographic evidences. The increase in Al_2O_3 might suggest accumulation of feldspar (sanidine) in the more acidic rocks (trachytic rocks). The scatter of Na_2O a n d K_2O f o r some samples could be related to alteration, but can also be related to the accumulation of nepheline and leucite respectively in these rocks. The Al_2O_3, N a $_2O$, and K_2O contents show a marked positive trend between SiO_2 = 45 and 50 wt.%, which could partly be due to the alteration of leucite and nepheline. This alteration probably occurred during the eruption of magma. An alternate reason for this trend is the buoyancy of leucite and its accumulation at the top of the magma chamber. CaO shows only minor variation from 9 to 13 wt.%, where the highest values indicate clinopyroxene accumulation.

The behavior of trace elements vs. silica is markedly different from that of the major elements (Fig. 8). All the samples show relatively similar Zr abundance (179–396 ppm) and in Zr vs. SiO_2 diagram, the rocks display a horizontal trend. The trachytic dikes/lavas have higher Zr content (656–805 ppm) (Appendix 3). The same trend is also clear for Nb values and the Nb abundance is N74 ppm in trachytic lavas/dikes and b45 ppm in other rock types (Appendix 3). This duality in Nb–Zr distributions might suggest a similar origin for all rocks types displaying horizontal trend except for the trachytic rocks which possess higher Zr–Nb values, reflected in the modal abundance of amphibole, phlogopite, zircon and apatite. Although Rb and Th show scatter, they show an overall increase with SiO_2 (Fig. 8). The trachytic rocks also posses higher Th content, and might reflect the incompatibility of this element resulting in accumulation in the fractionated melt (glass). La and Y show a general negative trend with SiO_2 but with much scatter. In general, amphibole and phlogopite are absent in silica undersaturated (leucite-bearing) ultrapotassic lavas, but present in silica saturated trachytic rocks. The shift from silica-undersaturated to silica-saturated rocks could be interpreted by early separation of more silica-undersaturated minerals like olivine and clinopyroxene and by the early crystallization of leucite. This feature associated with scattered trend in Harker diagrams (and/or linear trends) for some elements can

be interpreted also by contamination by crustal materials and/or mixing with compositionally different melt (Sorensen et al., 1999).

In contrast to major elements, REEs are more dependent on the mineralogy of the mantle source and hence reflect the process of melt formation and extraction (Hofmann and Jochum, 1996). Although the lavas are characterized by various modal mineralogy and relatively different signatures of major and some trace elements, they display similar chondrite-normalized REE patterns (Fig. 9). The rocks are all strongly enriched in light REE (136–474 times chondrite for La) relative to HREE (8–21 times chondrite for Yb; Fig. 9). The $La_{(n)}/Yb_{(n)}$ ratios vary between 13 and 40 for the Saray volcanic rocks and nepheline syenitic xenoliths. A high LREE/HREE ratio in the Saray high K-rocks could be related to the low degree of partial melting of an enriched mantle source. Partial melting of a garnet (−phlogopite) bearing mantle source could enrich LREE abundances relative to HREE (e.g., Zhang et al., 2008). Most of the Saray samples (although not all) have steep patterns from Ho to Yb, which might suggest the presence of residual garnet in the source of these magmas.

In primitive mantle-normalized diagram (Fig. 9), all the Saray high-K rocks are mainly characterized by strong enrichment in LILEs (e.g., Rb, Ba, U, K, and Th) relative to La. The lavas are characterized by conspicuous negative anomalies of HFSE including Nb, Ta and Ti relative to LREEs (Fig. 9). Phosphorous shows depletion in apatite-poor samples whereas a positive anomaly is displayed in apatite-bearing samples. Enrichment in LILE and depletion in HFSE are considered as main features of subduction-zone-related lavas (e.g., Pearce and Cann, 1973; Pearce, 1982; Pearce and Peate, 1995).

4.3. Sr–Nd–Pb isotope geochemistry

The Nd–Sr–Pb isotopic ratios of the Saray volcanic rocks are given in Table 1. The initial (11 Ma) $^{87}Sr/^{86}Sr$ ratio of these rocks varies between 0.70662 and 0.70797. Their initial $^{143}Nd/^{144}Nd$ ratio shows a narrow range between 0.51242 and 0.51252. All the Saray high-K volcanic rocks plot within the enriched quadrant of the conventional Nd–Sr isotope diagram (Fig. 10). The lavas show a tendency to EM2 OIB-mantle source with affinity to lamprophyres of the Alps (Fig. 10). The rocks show a distinct continental signature rather than the features of MORB and the Late Cretaceous ophiolitic lavas. The EM2 mantle signature is suggested to be inherited from recycling slab sediments (Zindler and Hart, 1986), although the origin of the EM2 signature could also involve metasomatism (i.e. melt/fluid infiltration) of both oceanic and continental lithosphere followed by recycling and long-term storage of this lithosphere (Workman et al., 2004).

The $^{206}Pb/^{204}Pb$ and $^{208}Pb/^{204}Pb$ values vary between 19.09 and 19.26 and 39.27 and 39.46 respectively (Table 1). The samples are characterized by highly radiogenic $^{207}Pb/^{204}Pb$ ratios, ranging from 15.69 to 15.70 (Fig. 10B). The lavas plot above the Northern Hemisphere Reference Line (NHRL; Hart, 1984), in both $^{207}Pb/^{204}Pb$ and $^{208}Pb/^{204}Pb$ diagrams (Fig. 10B,C). The highest $^{207}Pb/^{204}Pb$ and $^{208}Pb/^{204}Pb$ values are markedly higher than GLOSS and EM2 reservoir values (although $^{208}Pb/^{204}Pb$ ratio is between GLOSS and EM2) and indicate the involvement of subducted terrigenous sediments and/or continental crust in the source. These values could also correspond to an older reservoir of high-integrated Th/U.

5. Ar–Ar geochronology

The two sets of Ar–Ar age data yielded comparable ages on biotite grains for the Saray high-K trachytic lavas. The results are presented in Table 2 and plotted in Fig. 11. The $^{40}Ar–^{39}Ar$ data are presented in Appendix 5 together with a detailed discussion of each age. Laser step-heating experiments on biotite concentrates for two volcanic samples (E11-3 and E11-18) show the same ages.

Sample

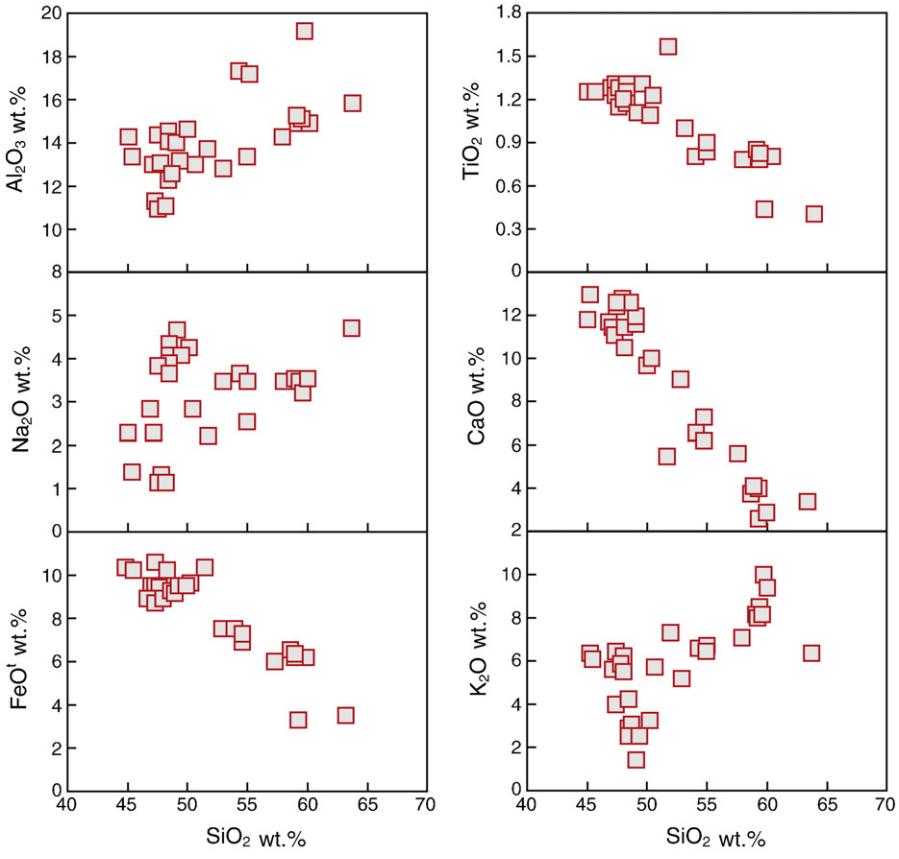

Fig. 8. SiO_2 variation diagrams for selected major elements of the Saray volcanic rocks.

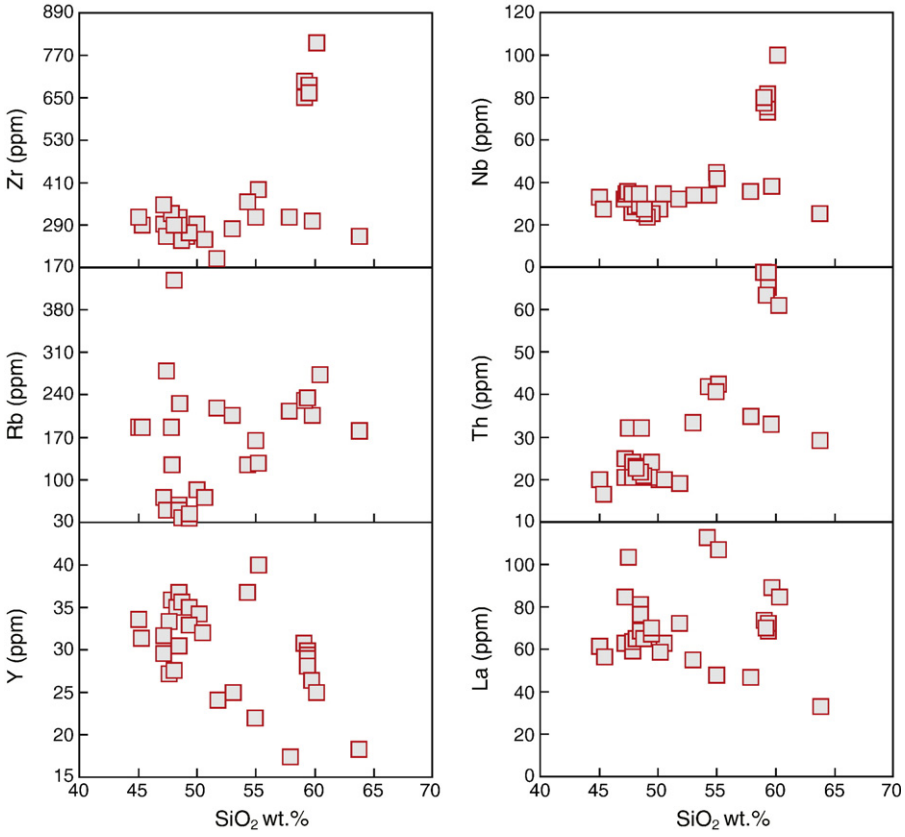

Fig. 8 (continued).

E11-3 displays a well-defined plateau age of 10.3± 0.10Ma. This age is indistinguishable from the isochron age of 10.3±0.17Ma (Table 2). The best age estimate of 10.9 ± 0.13 Ma for sample E11-18 comes from the plateau age which is comparable with the Ar–Ar isochron age of 10.7 ± 0.25 Ma.

6. Discussion

The origin and evolution of magmatic rocks along convergent plate margins involve a series of processes (e.g., Eyuboglu, 2013) including metasomatism of the mantle wedge by melt and/or fluids released by the downgoing slab (e.g., Pearce, 1982; Hawkesworth et al., 1991; Kelemen et al., 2004; Khedr et al., 2010), variable degree of partial melting of the metasomatized mantle (e.g., Pearce and Parkinson, 1993) and subsequent process at shallower depths such as magma mixing, AFC (e.g., DePaolo, 1981) and/or combinations of these processes (Ersoy et al., 2010). In this section we will briefly discuss the role of each process in the genesis of the high-K Saray lavas.

6.1. Subduction fingerprints of the Saray high-K volcanic rocks; arc-related setting?

The Saray high-K volcanic rocks are characterized by troughs in Nb, Ta, Ti and/or Zr (except the trachytes) and strong enrichment in incompatible elements including Rb, Ba, Th, U, K and LREE in a primary mantle-normalized diagram (Fig. 9). The enrichment in incompatible elements implies that the melt source was a metasomatized sub-continental lithospheric mantle (SCLM). The negative anomalies in Nb, Ta and Ti are typical features of subduction-related magmatism. A relatively high Sr/Y ratio, but also high Y content (resulting from clinopyroxene accumulation in most samples) is characteristic of the Saray volcanic rocks, different both from adakites and arc-like rocks (Fig. 12A). The influence of subduction components on the mantle source of the Saray volcanic rocks can also be detected in a Th/Yb vs. Ta/Yb diagram (Pearce, 1982) (Fig. 12B), where the rocks show high Th/Yb content (tending towards the value of average continental crust). This feature might suggest both subduction influence and/or crustal contamination of the lavas (AFC trend). The higher Th/Yb ratios also could indicate a lithospheric mantle source enriched by subduction components (Dilek et al., 2010). On the other hand, trachytic lavas have higher Th/Yb and Ta/Yb ratios than those of the other primary magmas, indicating that fractional crystallization also played an important role during the genesis of the rocks. The effect of fractional crystallization can be traced in Th/Yb vs. SiO_2 diagram (Fig. 12C), where the fractionated lavas (with higher SiO_2) have a higher Th/Yb ratio. The high LILE and LREE contents of the Saray lavas associated with radiogenic $^{207}Pb/^{204}Pb$ ratio are also similar to those of lavas formed in post-collisional setting (e.g., Turner et al., 1996; Zhao et al., 2009; Dilek et al., 2010).

There is a subtle but clear positive Nd anomaly in virtually all of these rocks, although this is not reflected in the REE patterns of most the alkalic rocks. The magmas that consistently show positive Nd anomalies are kimberlites and low-SiO_2 lamproites, including most leucite-bearing rocks. This feature could suggest that the parent magma(s) were not derived from a single-stage melting or crystallization process, but most likely reflects an early enrichment event when the LREEs were strongly enriched, followed by a melting event resulting in the selective removal of La, Ce and Pr. The distribution coefficients for the REE that define the Nd anomalies require garnet in the magma source. The depletion of Nb, Ta, and Ti clearly suggests that the dominant source of these magmas has been modified by subduction-related processes, or that a phase like rutile, that preferentially retains Nb, Ta, and Ti, is stable in the melt source. In the studied rocks, some trachytic rocks have negative P anomalies, whereas this anomaly is absent in the other rocks. This feature is apparently related to the apatite distribution, although the reasons remain vague.

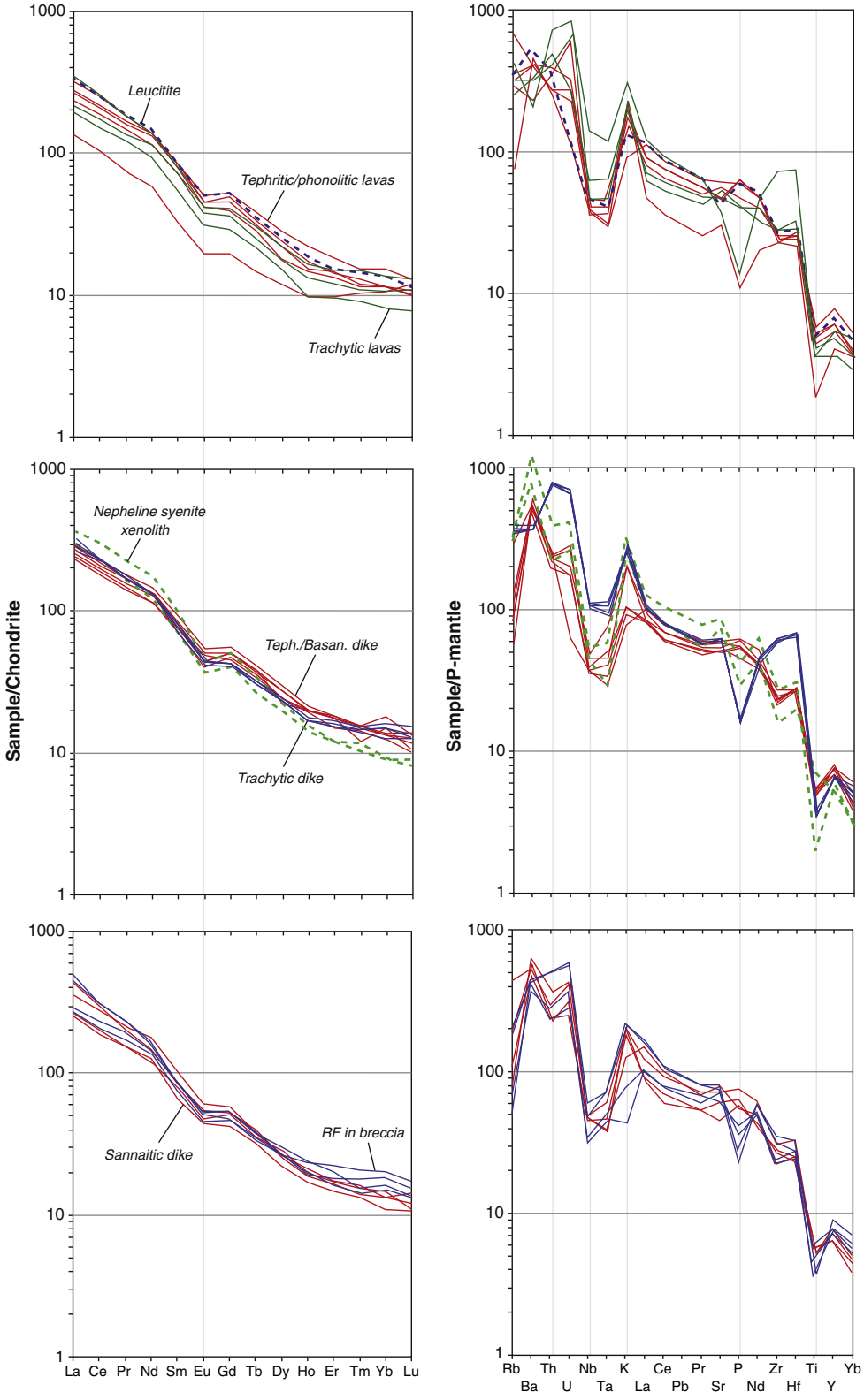

Fig. 9. Chondrite and primitive mantle-normalized rare earth and trace elements patterns for the Saray high-K rocks.

6.2. Petrogenetic model for the formation of high-K rocks: combination of various hypotheses

Chondrite- and primitive mantle-normalized REE and multi-element (Fig. 10), as well as Sr–Nd–Pb isotope (Fig. 10) diagrams indicate that the source region (s) of all these volcanic rocks is similar. The lavas have also the same ages as revealed by Ar–Ar dating results (Fig. 11). However, complex zoning of the clinopyroxene and other minerals in the Saray lavas associated with their major, trace (REE) and Sr–Nd–Pb isotopes suggest that different processes including fractional crystallization,

Table 1
Sr–Nd–Pb isotopes composition of the Saray high-K rocks.

Sample	Rb (ppm)	Sr ppm	Rb/Sr	$^{87}Rb/^{86}Sr$	$^{87}Sr/^{86}Sr$	Sm (ppm)	Nd (ppm)	Sm/Nd	$^{147}Sm/^{144}Nd$	$^{143}Nd/^{144}Nd$	$^{87}Sr/^{86}Sr$ (11 Ma)	$^{143}Nd/^{144}Nd$ (11 Ma)	eNd (11 Ma)	tCHUR (Ma)	U (ppm)	Th (ppm)	$^{206}/^{204}Pb$[a]	$^{207}/^{204}Pb$[a]	$^{208}/^{204}Pb$[a]
E11-6	268	816	0.3286	0.9508	0.707867	11.80	64.3	0.1835	0.1109	0.512423	0.707718	0.512415	−4.1	382.7	17.3	61.2	19.085531	15.699288	39.256970
E11-12	50	1250	0.0402	0.1162	0.707884	12.77	64.1	0.1992	0.1204	0.512484	0.707866	0.512475	−2.9	308.3	2.4	21.6	19.127086	15.697557	39.301117
E11-20	186	969	0.1917	0.5547	0.708055	12.00	61.9	0.1939	0.1172	0.512457	0.707968	0.512449	−3.4	347.7	4.8	23.7	19.109478	15.699000	39.280343
E11-26	233	1260	0.1847	0.5344	0.707670	11.92	62.2	0.1916	0.1159	0.512454	0.707587	0.512446	−3.5	347.8	14	68.5	19.146620	15.701650	39.303173
E11-29	50	1671	0.0296	0.0857	0.706631	12.96	68.5	0.1892	0.1144	0.512526	0.706618	0.512518	−2.1	207.9	9	32.1	19.258025	15.700302	39.462792
E11-36	129	1559	0.0827	0.2393	0.707846	13.59	79.1	0.1718	0.1039	0.512502	0.707809	0.512495	−2.5	223.9	12	42.5	19.153004	15.697985	39.335128
E11-44	122	1275	0.0958	0.2771	0.708117	12.10	56.3	0.2149	0.1299	0.512460	0.708074	0.512451	−3.4	406.9	6.6	20.3	19.140014	15.698164	39.280614
E11-58	186	1152	0.1613	0.4666	0.707708	11.79	60.4	0.1952	0.1180	0.512514	0.707635	0.512506	−2.3	240.7	5.5	19.9	19.192281	15.700180	39.358714

[a] Due to the lack of Pb values in whole rock data, all Pb isotopes are present-day values.

assimilation–fractional crystallization and/or magma mixing could have played important roles during their formation.

6.2.1. Fractional crystallization: subordinate mechanism for the evolution of the Saray rocks?

The trends displayed by major and trace elements in Harker diagrams (Fig. 8) suggest that fractional crystallization was predominant during the formation of the Saray high-K rocks. Whereas Zr should show enrichment during fractionation (with increasing SiO_2) in the present case, all the samples display relatively similar Zr abundance except for trachytic dikes/lavas that have high Zr content. This is also true for Nb. Y shows lower values with highest SiO_2 for trachytic rocks which might reflect clinopyroxene (and amphibole) fractionation. The other samples record clinopyroxene accumulation with higher Y content. All the samples display negative Eu anomalies. Because most of the samples in this study do not contain amphibole (the only other phase that combined with apatite, could potentially produce Eu anomalies), the negative Eu anomaly probably derives from fractional crystallization of feldspars, and this indicates that none of the rocks represents a “primary” magma composition that reflects a melt from a mantle source. The nature of the negative Eu anomalies suggests that the rocks evolved by fractional crystallization, and did not originate from partial melting in the presence of feldspar in the source. For most mafic alkalic rocks, the pressure of melting is probably above the stability range of feldspars (~10 kb), so that the Eu anomaly is unlikely to be formed during partial melting. As mentioned earlier, the shift from silica-undersaturated to silica-saturated rocks could be also interpreted by early separation of more silica-undersaturated minerals such as olivine and clinopyroxene and by early crystallization of leucite. The effect of fractional crys-tallization is also displayed in a Th/Yb vs. SiO_2 diagram (Fig. 12C). The major elements define an apparent liquid line of descend, although most of the incompatible trace elements do not show the behavior of a typical fractionating system. Thus, fractional crystallization alone cannot explain the other features of these rocks including the complex oscillatory zoning of pyroxene and/or their isotopic characteristics. Other mechanisms such as AFC and/or magma mixing should also be considered.

6.2.2. Assimilation-fractional crystallization processes (AFC): an alternate mechanism?

Assimilation and fractional crystallization processes are common in most Anatolian high-K rocks (e.g., Gulec, 1991; Aldanmaz et al., 2000; Yılmaz et al., 2001; Dilek et al., 2010; Ersoy et al., 2010; Eyuboglu, 2010). Th/Yb vs. Ta/Yb relationships of the Saray lavas and their radiogenic $^{207}Pb/^{204}Pb$ ratio also show the effect of both fractional crystallization (FC) and assimilation-fractional crystallization (AFC) processes. In order to evaluate the effect of AFC, we used the FC–AFC–FCA and mixing modeler software of Ersoy and Helvaci (2010). Sample E11-29 having the lowest SiO_2 and relatively high MgO (with both low LOI and $^{87}Sr/^{86}Sr$ ratio) is assumed to represent the starting magma composition for AFC modeling. An average fractionating composition of plagioclase (65%) + clinopyroxene (15%) + amphibole (10%) + biotite (10%) following Ersoy et al. (2012a) is used (Fig. 13), except in Fig. 13E where the starting composition used was that of sample E11-58 with fractionating mineral assemblage of plagioclase (40%) + clinopyroxene (30%) + amphibole (10%) + biotite (10%) + olivine (10%). These con-siderations also fit well with our observations in the field showing clinopyroxene–phlogopite–feldspar (±olivine) cumulate-like autholites in pyroclastic deposits. The metamorphic rocks (granitic gneiss; sample CHJ09-12) of the Chah-Jam complex from central Iran with Cadomian age (ca. 550 Ma; Shafaii Moghadam et al., unpublished data), are considered as assimilant in the mid-crustal level, exhumed during the extension phases in the late Cretaceous in Iran (Hassanzadeh et al., 2008). These rocks have the same ages and similar mineral assemblages to those of the Cadomian granitic gneisses that host the high-K Saray volcanic rocks. The partition coefficients and the composition of starting

material and assimilant in FC and AFC models are given in Tables 3 and 4. The interaction of the starting melt with the assimilant will result in an increase of $^{87}Sr/^{86}Sr$ and decrease in $^{143}Nd/^{144}Nd$ of the contaminated magma (Pb values are not available in the case of assimilant; sample CHJ09-12, to model the AFC using Pb isotopes). To test the effect of contamination of the Saray lavas with mid-crustal rocks (as evidenced by Chah-Jam metamorphic rocks; CJMR), the $^{87}Sr/^{86}Sr$ and $^{143}Nd/^{144}Nd$ ratios of the volcanic rocks are plotted against Th and Sr and also vs. the Sr/Rb ratio (Fig. 13). The trend of the AFC model best explains the $^{143}Nd/^{144}Nd$ vs. Sr/Rb and Sr compositions of the Saray volcanic rocks using the CJMR as assimilant and low (r = 0.2) to medium (r = 0.4) degrees of assimilation, and the trends displayed by $^{87}Sr/^{86}Sr$ ratio vs. Th and Sr. As minor olivine is present in the Saray primitive lavas (and in autholites within the pyroclastic rocks), we consider another fractionating mineral assemblage of plagioclase (40%) + clinopyroxene (30%) + amphibole (10%) + biotite (10%) + olivine (10%) (with CJMR as assimilant) and using V/Y vs. Th to test the contamination effect. The strongest positive correlation is achieved by this model and using ratios of assimilation to crystallization (r) from 0.2 to 0.8 (Fig. 13E). Although the effects of contamination can be traced among the Saray volcanic rocks, especially in the case of the V/Y vs. Th plot, the petrographic and geochemical features of the lavas such as the presence of both Ti–Al rich and Ti–Al poor Cpx phenocrysts in same rocks, complex zoning of the clinopyroxenes (and other phases), high $^{87}Sr/^{86}Sr$ values, and the high abundances of LREEs and LILEs cannot be explained either by FC or by AFC processes. In addition, the content of incompatible trace elements in the Saray rocks is higher than that of crustal end member, suggesting that crustal contamination would have diluted rather than enriched the trace element content of the Saray magmas. Therefore other factors including mantle source heterogeneity due to the metasomatic events relating to sediment fluids/melts from descending slab and/or different degrees of partial melting of the metasomatized mantle should also be considered.

6.2.3. Source heterogeneities and mixing; a more favorite mechanism?

Post-collisional magmatic rocks with shoshonitic and ultra-potassic (with high K and/or high MgO and with different degree of silica saturation/undersaturation) signatures are abundant in the Mediterranean–Iran regions, and their origin has been correlated to partial melting of clinopyroxene–amphibole–phlogopite veins in a metasomatized mantle source (e.g., Gulec, 1991; Prelević et al., 2004, 2005, 2008; Ersoy et al., 2008; Conticelli et al., 2009; Pe-Piper et al., 2009; Conticelli et al., 2012 and references therein). Their genesis is suggested to be related to recycling of pelitic sediments and subsequent K-metasomatism and enrichment of peridotitic lithosphere (e.g., Conticelli et al., 2012). Factors that control the silica activity of the high-K melts are suggested to be related to: 1 — abrupt change of the com-position of the recycled sediments (e.g., Conticelli and Peccerillo, 1992; Frezzotti et al., 2009) a n d / o r 2 — interaction between deep asthenos-pheric mantle with lithospheric portion of mantle wedge through slab tears within the descending slab (e.g., Conticelli et al., 2012; Prelević et al., 2012). From petrographic and geochemical evidence, it is clear that some mixing between newly supplied silica under-saturated magma and batches of pre-existing calc-alkaline magmas might have occurred during the evolution of the Saray volcano.

At convergent margins, the composition of the mantle wedge can be modified by the addition of subduction-related components such as melts and/or fluids released from the subducting slab (sediments and/or underlying MORB-type basalts) (e.g., McCulloch and Gamble, 1991; Hawkesworth et al., 1997). Some elements are highly mobile in fluids such as LILEs whereas others such as Th and LREEs are enriched in sediments and can be concentrated in sediment-derived melts. We attempted to model the effects of sediment fluids (SF) and sediment melts (SM) on the mantle wedge (primary mantle; PM) using ratios like as Th/Nb vs. Ba/Nb and Ce/Yb vs. Sr/Yb (Fig. 14A,B). The Saray high-K rocks are characterized by elevated Th/Nb but variable Ba/Nb ratios. A higher Ba/Nb ratio could be interpreted as evidence for higher degree of sediment-derived fluid contribution rather than sediment melts (if we neglect the probable Ba mobility during alteration). However the Saray rocks have elevated Ce/Yb and Sr/Yb ratios, mostly compatible with sediment melt (SM) components. Higher Sr/Yb and Ce/Yb could also reflect the effect of residual garnet in the mantle source (Ersoy et al., 2010). The presence of a sediment-derived, subduction-related metasomatic component with high Sm/La and Th/La ratios (i.e., SALATHO; Tommasini et al., 2011) is suggested to be responsible for formation of the Mediterranean lamproites (e.g., Conticelli et al., 2011; Tommasini et al., 2011; Conticelli et al., 2012). However in the Saray volcano, the trachytic dikes have a higher Th/La ratio and indeed, these rocks are compositionally different from lamproites by having lower Mg# and higher Al_2O_3. The SALATHO component is interpreted to derive from melting of accreted mélange during the collision of the Gondwana-derived continental blocks with Eurasia associated with the closure of Neotethyan oceanic basins (Tommasini et al., 2011).

Small mantle wedge heterogeneity, as described for Mediterranean high-K rocks (e.g., Conticelli and Peccerillo, 1990; Foley, 1992; Conticelli et al., 2012), involving the interaction between calc-alkaline and lamproite-like (ultrapotassic) components could be responsible for the genesis of the Saray lavas. In this model, the ultrapotassic component is related to a metasomatized mantle with vein networks whereas the calc-alkaline component is derived from the mantle surrounding the vein networks (e.g., Foley, 1992; Perini et al., 2004; Bianchini et al., 2010). Both components are present in the same lithospheric mantle. The calc-alkaline and ultrapotassic melts responsible for the Saray high-K rocks could have been produced at the same time from different mantle source levels and mixed in upper levels within crustal magma chambers. The presence of metasomatized mantle with vein networks reinforces the chemical effects of SM and SF addition on the PM-like mantle source. In order to estimate the amount of the subducted sediment contribution to the mantle source of the Saray volcanic rocks, we used their Sr–Nd isotopic ratio, compared with other end-members including primary mantle and subduction components (Fig. 14C,D). In this diagram, the mixed mantle source (MMS) is obtained from 10% mixing of PM with a subducted sediment component (Ersoy et al., 2010). On the Sr–Nd isotope diagram (Fig. 14C), the Saray volcanic rocks define a binary mixing trend, representing 5–8% mixing between the primary mantle (PM) and sediment melts. A sedimentary component in late Miocene Saray volcanic rocks is also evidenced from Pb isotopes data of the lavas (Fig. 10). Both Fig. 10A and B suggest that this is the contribution from an old source. Particularly, the elevated $^{207}Pb/^{204}Pb$ requires an old source (i.e., a source from where the decay of ^{235}U generated high ^{207}Pb, and which was subsequently isolated from mixing with the younger component). The Pb isotope data in Fig. 10B are consistent with similar data from Turkey (e.g., Prelević et al., 2012), showing compositions that are offset to the high side of NHRL and this is a regional pattern.

The highly radiogenic $^{87}Sr/^{86}Sr$ and $^{207}Pb/^{204}Pb$ values for the Saray lavas are also another robust evidence for the involvement of slab sediments. Melting of subducted sediments might have supplied the crustal components to the mantle source of the Saray volcanic rocks (e.g., Prelević et al., 2005, 2012; Conticelli et al., 2012). The Saray lavas, like most of the Mediterranean lamproites, plot in the mixing trend between melts derived both from high Nb/U as well as less radiogenic Sr source (mantle component 2) and melts generated from a mantle contaminated by subducted sediments and/or crust-derived sedi-mentary materials with low Nb/U and radiogenic Sr isotope (mantle component 1; Fig. 14D) (Prelević et al., 2012). Prelević et al. (2012) suggested that this addition should be as sediment partial melt patches, evidenced by high Th/Nb and/or Th/Yb ratios. The mantle component 1 is characterized by highly radiogenic $^{87}Sr/^{86}Sr$ and $^{207}Pb/^{204}Pb$, non-radiogenic $^{143}Nd/^{144}Nd$ and a relatively non-radiogenic $^{206}Pb/^{204}Pb$. The continental crustal component in the Saray high-K rocks is inferred to have originated from turbiditic sediments as indicated by the very high $^{87}Sr/^{86}Sr$ and $^{207}Pb/^{204}Pb$. The $^{207}Pb/^{204}Pb$, $^{208}Pb/^{204}Pb$

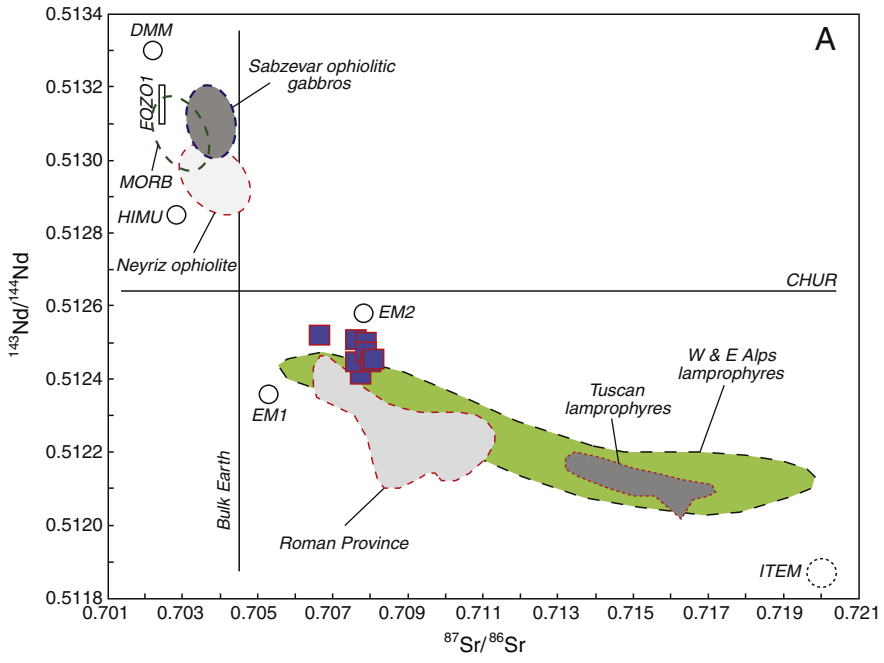
A
DMM
FOZO1
MORB
HIMU
Neyriz ophiolite
Sabzevar ophiolitic gabbros
CHUR
EM2
EM1
Bulk Earth
W & E Alps lamprophyres
Tuscan lamprophyres
Roman Province
ITEM
143Nd/144Nd
87Sr/86Sr
0.5134
0.5132
0.5130
0.5128
0.5126
0.5124
0.5122
0.5120
0.5118
0.701
0.703
0.705
0.707
0.709
0.711
0.713
0.715
0.717
0.719
0.721

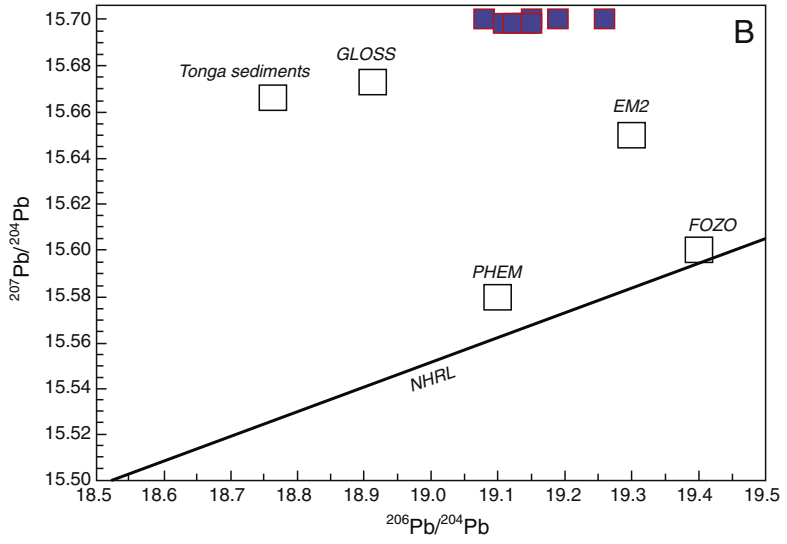
B
Tonga sediments
GLOSS
EM2
FOZO
PHEM
NHRL
207Pb/204Pb
206Pb/204Pb
15.70
15.68
15.66
15.64
15.62
15.60
15.58
15.56
15.54
15.52
15.50
18.5
18.6
18.7
18.8
18.9
19.0
19.1
19.2
19.3
19.4
19.5

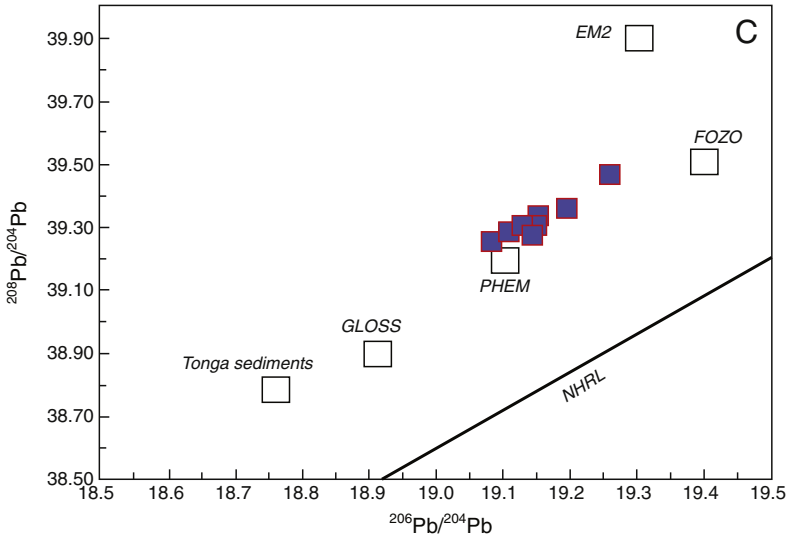
C
EM2
FOZO
PHEM
GLOSS
Tonga sediments
NHRL
208Pb/204Pb
206Pb/204Pb
39.90
39.70
39.50
39.30
39.10
38.90
38.70
38.50
18.5
18.6
18.7
18.8
18.9
19.0
19.1
19.2
19.3
19.4
19.5

Table 2
Summary of $^{40}Ar/^{36}Ar$ ages for trachytic lavas.

Sample	Rock	Material dated	Plateau age (Ma)	Isochron age (Ma)	$(^{40}Ar/^{36}Ar)_i$[a]	MSWD/n[b]
E11-3	Trachytic lava	Biotite	10.33 ± 0.10 Ma	10.32 ± 0.17 Ma	312 ± 27	1.39/13
E11-18	Trachytic lava	Biotite	10.93 ± 0.13 Ma	10.68 ± 0.25 Ma	305 ± 8	0.42/9

[a] Initial ($^{40}Ar/^{36}Ar$) calculated from the intercept of the best straight line defined with the data in the ($^{36}Ar/^{40}Ar$) vs. ($^{39}Ar/^{40}Ar$) correlation diagram.
[b] Goodness of fit of the best straight line and number of points used.

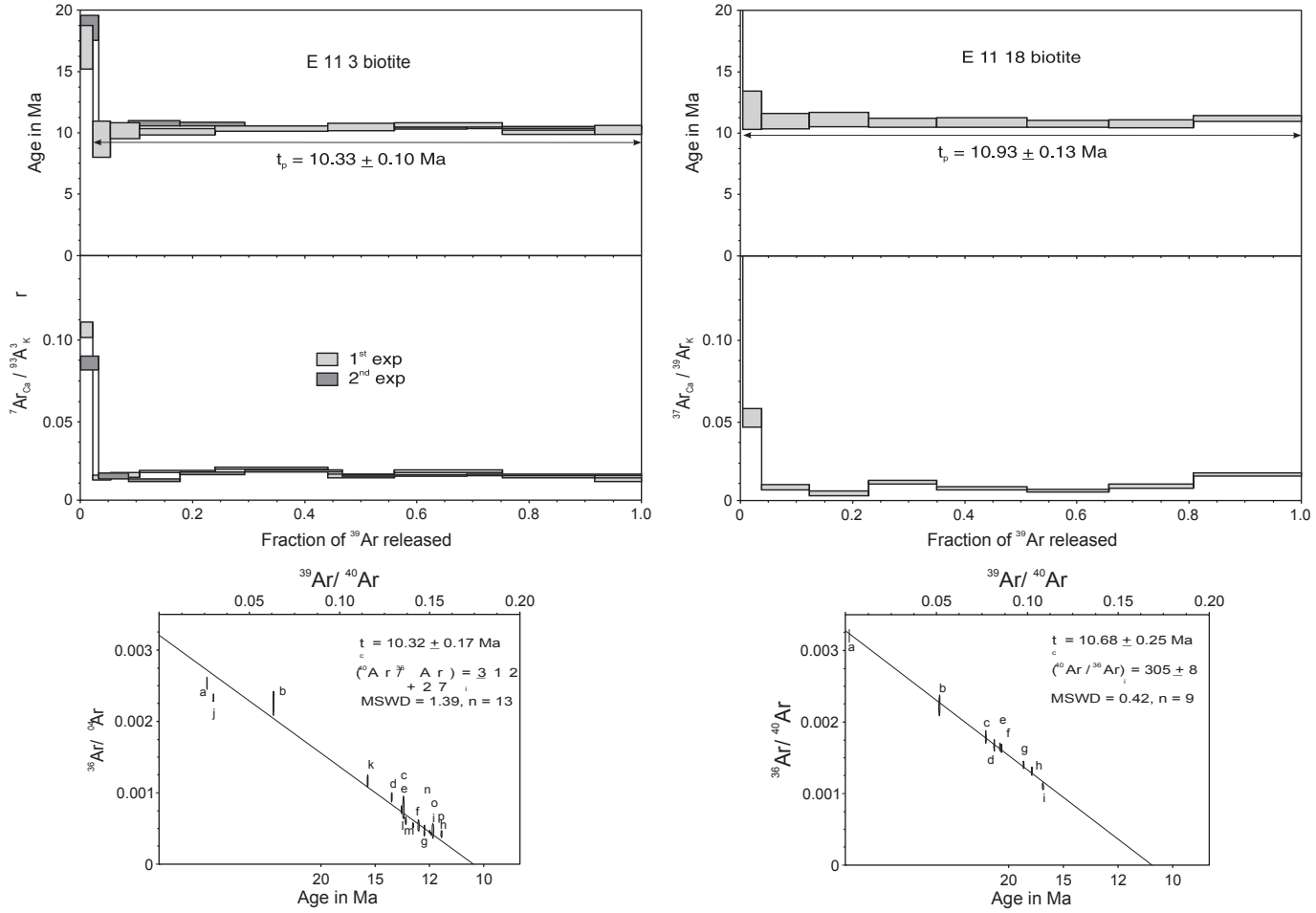

Fig. 11. Age spectra and $^{36}Ar/^{40}Ar$ vs. $^{39}Ar/^{40}Ar$ correlation diagrams for the Saray trachytic lavas. In the age spectra, the weighted mean of the fractions close to the arrow, were used to calculate the plateau age.

and $^{206}Pb/^{204}Pb$ isotopes ratios of the Saray lavas are higher than those of global subducting sediments (GLOSS) and enriched mantle II (EM2). The Saray samples have a (near to-) super chondritic Hf/Sm ratio, indicating that the subducted sediments had terrestrial origin. This is also well constrained from the $^{207}Pb/^{204}Pb$ ratio. The lavas might thus reflect the involvement of subducted terrestrial sediments and/or continental crust in the mantle sources, which have either high Nd/Hf (pelagic sediment) or low Nd/Hf (terrestrial sediments and/or continental crust) (e.g., Gasparon and Varne, 1998; Plank and Langmuir, 1998; Carpentier et al., 2009; Handely et al., 2011; Shafaii Moghadam et al., 2012).

6.2.4. Non-modal dynamic melting of metasomatized mantle source

Decompression melting of metasomatized lithospheric lherzolite with minor phlogopite and pargasite has been invoked for the formation of primary high-K magmas by dehydration melting at ~1 GPa, 1050–1150 C° (Conceição and Green, 2004). In order to model the partial melting

Fig. 10. (A) $^{143}Nd/^{144}Nd$ vs. $^{87}Sr/^{86}Sr$ ratios for the Saray high-K rocks compared with the mantle components HIMU, EM1, EM2, DMM (after Zindler and Hart, 1986); FOZO1 (after Hart et al., 1992) and ITEM (after Bell et al., 2004); present-day Bulk Earth and CHUR (chondritic uniform reservoir) are also shown. Most of the data display cluster close to the EM2. The Eastern and Western Alps and Tuscan lamprophyres and Roman Province fields are from Bell et al. (2013); Data for Neyriz lavas and Sabzevar ophiolite gabbros are from Shafaii Moghadam et al.(unpublished data). Note that Neyriz ophiolitic lavas have a shift towards higher $^{87}Sr/^{86}Sr$ ratio due to the reaction with seawater; (B) $^{207}Pb/^{204}Pb$ vs. $^{206}Pb/^{204}Pb$ and (C) $^{208}Pb/^{204}Pb$ vs. $^{206}Pb/^{204}Pb$ diagrams for the Saray lavas. GLOSS = globally subducting sediments (Plank and Langmuir, 1998); PHEM = primitive helium mantle (Farley et al., 1992).

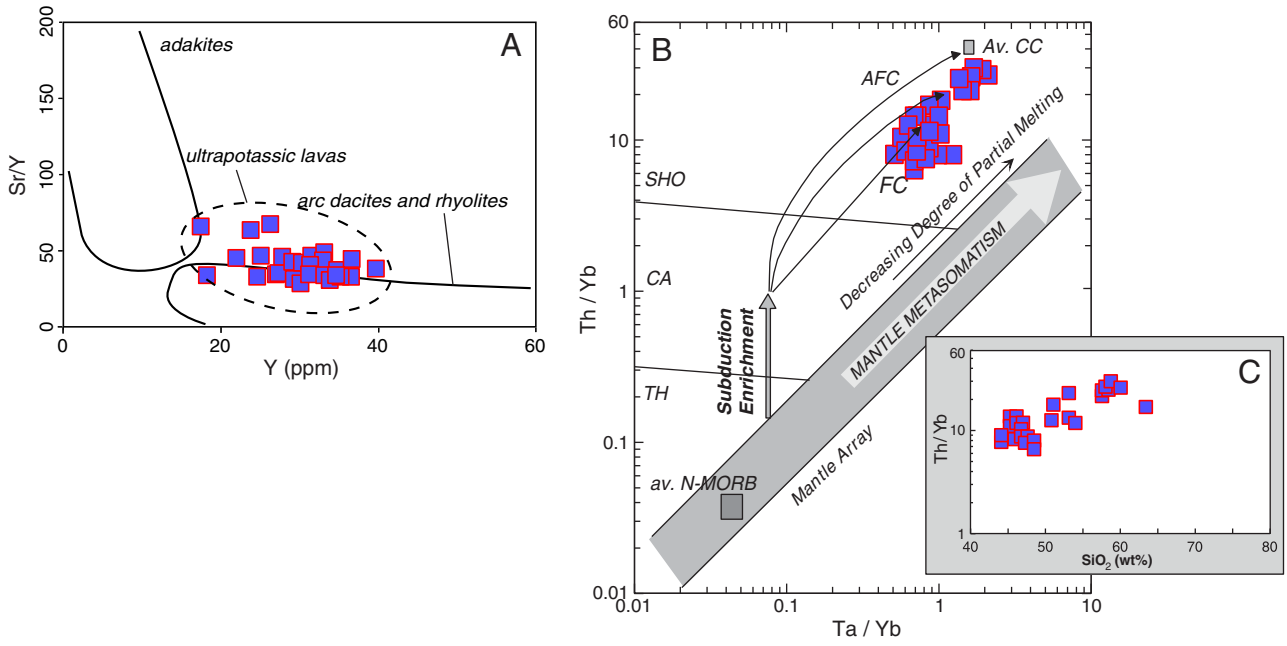

Fig. 12. (A) Sr/Y vs. Y diagram for discriminating adakites from arc dacites and rhyolites. The Saray high-K volcanic rocks have high Sr/Y ratio but low Y content; (B) Th/Yb vs. Ta/Yb diagram (Pearce, 1982) diagram showing high Th/Yb ratio for the Saray volcanic rocks which displays a lithospheric mantle source enriched by subduction components; (C) Th/Yb vs. SiO_2 plot for the Saray rocks showing the effect of fractional crystallization (SiO_2 increasing) on Th/Yb ratio.
The fields for adakite and normal island-arc dacites and rhyolites are based on the works of Defant and Drummond (1990, 1993), and Castillo et al. (1999).

trajectories, the mineralogical composition of the mantle source (associated with the partial melting degree of this mantle), from which the Saray volcanic rocks originated are inferred as shown in Fig. 15. Non-modal dynamic melting of a garnet-bearing amphibole lherzolite with Ulten Zone Peridotite (UZP), Eastern Alps (Rampone and Morten, 2001) composition (see Table 5) is modeled on Tb/Yb vs. La/Yb and Tb/Yb vs. Th/Yb diagrams (Fig. 15). The UZP is suggested to represent a paleo-mantle wedge formed above a subducted continental slab (Rampone and Morten, 2001). On this plot, the partial melting trajectories of UZP with variable garnet (5%, 7% and 10%) are shown. In Tb/Yb vs. La/Yb diagram, the samples do not follow the melting trends of UZP mantle source whereas most of the primary lavas plot between 6 and ~8% partial melting of garnet lherzolite source of Walter (1998). In the Tb/Yb vs. Th/Yb diagram, the primary samples do not follow the melting trajectory of the garnet lherzolite (Walter, 1998). The samples have higher a Th/Yb ratio, probably resulting from the AFC process during ascent of the Saray melts (see Fig. 13E) and/or addition of high sediment melt input into the mantle wedge (Fig. 14A). The scatter of the samples in these diagrams seems to be the result of mixing between melts produced by different sources or by the same batch of melt passing through a compositionally-zoned mantle during multiple stages of partial melting and melt migration (Ersoy et al., 2010; Ersoy et al., 2012a,b). This interpretation is well constrained by the complex zoning of clino-pyroxenes of the lavas. Trace (and REE) elements of the clinopyroxene from the Saray lavas in future studies could help to better understand this process.

Melting of phlogopite and apatite-bearing peridotites in the sub-continental lithospheric mantle is also proposed for the genesis of the Saray high-K rocks (Pang et al., 2013). However, our modeling (not shown) using both dolomite-bearing garnet peridotites (sample ULT18; Sapienza et al., 2009) and phlogopite-rich peridotites (MADRID; Gregoire et al., 2002 and/or Finero phlogopite harzburgite; Hartmann and Wedepohl, 1993) indicates that neither of these could produce the Saray ultrapotassic rocks. As phlogopite (and pargasite)-bearing lherzolites are suggested to be the source for the ultrapotassic lavas in the Anatolian regions (e.g., Prelević et al., 2012), it is possible that the phlogopite signature decreased through mixing of melts derived from different mantle sources (mantle components 1 and 2). This hypothesis is well constrained from complex oscillatory zoning of the Saray clinopyroxenes.

6.3. Geodynamic implications

Potassium-rich magmatic rocks occur widely in different tectono-magmatic environments such as continental active margins, post-collisional magmatic arcs and within plate settings (e.g., Muller et al., 1992; Mitchell et al., 1994; Elitok et al., 2010; Eyuboglu, 2010; Lu et al., 2012). It is widely accepted that the late Cenozoic magmatism in the Mediterranean–Iran regions occurred in a post-collisional setting and resulted from partial melting of a subduction-related metasomatized sub-continental lithospheric mantle (e.g., Aldanmaz et al., 2000; Alici Sen et al., 2004; Altunkaynak and Genç, 2008; Ersoy et al., 2010; Altunkaynak et al., 2012; Ersoy et al., 2012a,b; Prelević et al., 2012). Most of the high-K rocks from the Anatolian plateau are thought to have been derived from partial melting of a mantle source similar to UZP, either contaminated by multi-stages of oceanic subduction events during a long period and/or contaminated by continental subduction (Ersoy et al., 2010, 2012a,b). In the latter case, the deep subduction of upper continental crust might have led to metasomatism of the mantle by K-rich fluids (Schreyer et al., 1987). This process is mostly responsible for the genesis of lamproites. The Saray lavas are enriched in LILEs and LREEs relative to primary mantle and mark the presence of crustal components. This is also well constrained by more radiogenic $^{87}Sr/^{86}Sr$ and $^{207}Pb/^{204}Pb$ ratios for the Saray lavas. These features suggest that the Saray post-collisional late Miocene magmas were derived from small degrees of partial melting of subduction-metasomatized (subcontinental) lithospheric mantle source. However, mixing of melts from the two types of mantle source is suggested based on the isotopes and trace elements ratios (e.g., Fig. 15). This scenario is well consistent with those of the other post-collisional magmatic rocks from the Miocene to Quaternary in the Turkish–Iranian High Plateau (e.g., Pearce et al., 1990; Keskin et al., 1998; Yilmaz et al., 1998; Dilek et al., 2010; Eyuboglu et al., 2012). Slab break-off and/or partial delamination (due to the roll-back of the subducting Tethyan lithosphere) of the

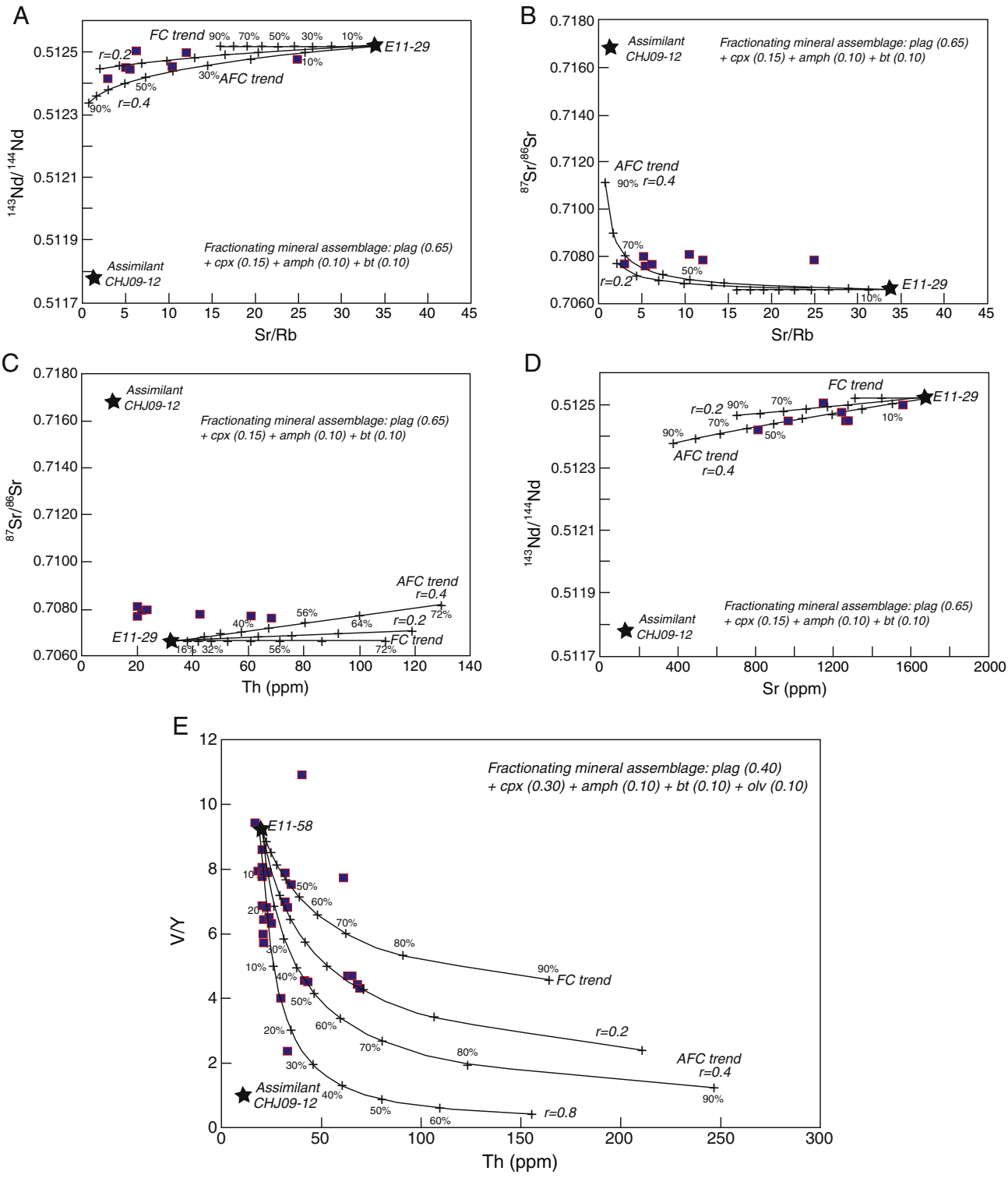

Fig. 13. $^{143}Nd/^{144}Nd$ vs. Sr/Rb (A), $^{87}Sr/^{86}Sr$ vs. Sr/Rb (B), $^{87}Sr/^{86}Sr$ vs. Th (C) and $^{143}Nd/^{144}Nd$ vs. Sr (D) with modeled FC and AFC (r = 0.2 and 0.4) curves to model the assimilation–fractional crystallization pathways between an high-K lava (sample E11-29) and a granitic gneiss from Chah-Jam metamorphic complex (central Iran, Shafaii Moghadam et al., 2013). An average fractionating composition of plagioclase (65%)+ clinopyroxene (15%)+amphibole (10%)+Biotite (10%) according to Ersoy et al.'s (2012a) suggestion is used in these models;(E) Different pathways for FC and AFC modeling with an basanitic dike (sample E11-58) as starting composition with fractionating mineral assemblage of plagioclase (40%) + clinopyroxene (30%) + amphibole (10%) + biotite (10%) + olivine (10%).

mantle lithosphere associated with partial melting of clinopyroxene–amphibole–garnet (and/or phlogopite) rich metasomatic veins in the lithospheric mantle in a post-collisional setting has been suggested as likely processes (Dilek et al., 2010). In this model, the first batch of lavas were derived mainly from the metasomatic veins and are mostly ultrapotassic as compared to the later high-K calc-alkaline and/or shoshonitic products which were suggested to be have resulted from melting of veins surrounding peridotites (Ersoy et al., 2010; Conticelli et al., 2012). However this model is not favorable for the Saray rocks as they have identical ages (~11 Ma) and nearly the same geochemical patterns. On the other hand, the mantle source of the Saray lavas is different from amphibole- (and/or phlogopite-) bearing lherzolites as

Table 3
Partition coefficients used in FC, AFC and melting models. (after Ersoy et al., 2010; Ersoy and Helvaci, 2010).

Elements	Olivine	Opx	Cpx	Garnet	Amphibole	Biotite	Plagioclase
Cs	0.0004	0.01	0.13	0.003	0.046	0.626	0.13
Rb	0.002	0.003	0.0047	0.042	0.1	5.18	0.1
Ba	0.002	0.002	0.00061	0.023	0.45	3.48	0.3
Sr	0.00217	0.007	0.0963	0.012	0.45	0.183	2
Th	0.04	0.13	0.03		0.05	0.0145	0.01
U	0.045	0.035	0.04	0.015	0.08	0.0011	0.01
Zr	0.0045	0.03	0.121	0.3	0.4	0.0232	0.048
Hf	0.0037	0.055	0.263	0.3	0.5	0.19	0.051
Ti	0.011	0.024	0.1	0.1	0.69	0.9	0.04
Ta	0.000018	0.15	0.013	0.06	0.25	0.1069	0.04
Y	0.0038	0.2	0.438	2	1.1	0.007	0.03
Nb	0.0017	0.15	0.0027	0.1	0.3	0.0853	0.01
Sc	0.68	1.2	3.2	2.6	4.2	8.3	0.04
Cr	0.7	10	34	0.6	34	5.4	0.08
Ni	29	5	14	5.1	6.8	1.3	0.04
V	0.8	0.6	1.35		1.35		0.022
La	0.00064	0.002	0.0435	0.01	0.2	0.035	0.27
Ce	0.0005	0.003	0.0843	0.021	0.35	0.03	0.2
Pr	0.0008	0.0048	0.124	0.054	0.35	0.035	0.17
Nd	0.001	0.0048	0.173	0.087	0.65	0.04	0.14
Sm	0.0013	0.01	0.283	0.217	0.85	0.03	0.11
Eu	0.0016	0.013	0.312	0.32	0.8	0.04	0.73
Gd	0.0015	0.016	0.336	0.498	0.95	0.03	0.066
Tb	0.0015	0.019	0.364	0.75	1.2	0.03	0.06
Dy	0.0017	0.022	0.363	1.06	1.3	0.035	0.055
Ho	0.0016	0.026	0.378	1.53	1	0.03	0.048
Er	0.0015	0.03	0.351	2	0.9	0.03	0.041
Tm	0.0015	0.04	0.297	3	0.9	0.03	0.036
Yb	0.0015	0.049	0.313	4.3	0.8	0.04	0.031
Lu	0.0015	0.06	0.265	5.5	0.8	0.03	0.025

partial melting models do not support this type of source. In contrast to the NW Iran region, the distribution of the ultrapotassic rocks with lamproitic composition in the Eastern Turkish region, within the Turkish–Iranian high Plateau domain, maybe related to the presence of a thicker lithosphere in NE Turkey and hence earlier collision between Arabia and Anatolian plate.

Collision between the Arabian and Anatolian plates began at about the time when Arabia separated from Africa ~25 Ma ago (Shafaii Moghadam and Stern, 2011). A wide variety of geological responses to "Chilean-type" subduction of the Arabian passive margin and continental crust have been documented, including: (1) development of a foreland basin in the Zagros during the Oligocene (Hempton, 1987; Beydoun et al., 1992); (2) Early to mid-Miocene transition from marine to non-marine sedimentation throughout Iran (Dercourt et al., 1986; Sengor and Natalin, 1996); (3) a latest Miocene/Pliocene influx of coarse clastics into the foreland basin, along with rapid subsidence of the Caspian Sea (Beydoun et al., 1992; Allen et al., 2002); and (4) a major change in the Urumieh–Dokhtar arc magmatic activity that occurred at about this time. Eruptions diminished and changed from calc-alkaline to shoshonitic or even alkaline in Oligocene–Miocene upward. Continental collision led to slab-break-off and development of an asthenospheric window, facilitating partial melting of the subduction-contaminated sub-continental lithospheric mantle and generating the high-K rocks as well as adakites in the region (Agard et al., 2005; Dilek et al., 2010). Melting of the sub-continental lithospheric mantle (SCLM) could be related to thermal perturbation of the SCLM caused by partial removal of the lithospheric roots in a post-collisional setting (e.g., Aldanmaz et al., 2000; Zhao et al., 2009; Ersoy et al., 2010, 2012a,b; Prelević et al., 2012). The shift from Late Miocene shoshonitic and high-K magmatism (lithospheric signature) to Quater-nary OIB-like (asthenospheric signature) lavas is common in NW Iran (e.g., Dilek and Altunkaynak, 2009; Kheirkhah et al., 2009; Dilek et al., 2010), although shoshonitic volcanism also occurred widely during the

Table 4
The parameters used in FC, AFC, mixing and melting models (After Ersoy et al., 2010).

Element	Primitive mantle (PM)	Sediment melt (SM)	Sediment fluid (SF)	Mixed mantle source (MMS)	Assimilant (CHJ09-12)	Starting melt (E11-29)
Rb	0.605	89.46	28.67	6.45	104.50	49.50
Ba	6.750	1173.63	922.93	110.90	698.00	4410.00
Sr	20.300	436.56	411.37	60.67	140.50	1671.40
Th	0.083	8.69	1.44	0.58	11.55	32.10
Y	4.370	8.27	25.71	5.63	48.00	33.20
Nb	0.588	7.00	3.38	1.05	14.30	36.00
La	0.686	17.88	7.23	1.87	28.90	102.70
Ce	1.786	34.73	14.34	4.06	59.50	181.50
Nd	1.327	12.32	5.34	1.83	28.70	68.50
Sm	0.431	2.07	2.41	0.61	6.19	12.96
Yb	0.462	0.78	2.60	0.58	5.10	2.39
V					46.00	230.00
$^{87}Sr/^{86}Sr$	0.704500	0.710116	0.710116	0.708425	0.716805	0.706618
$^{143}Nd/^{144}Nd$	0.512640	0.512150	0.512150	0.512469	0.511776	0.512518

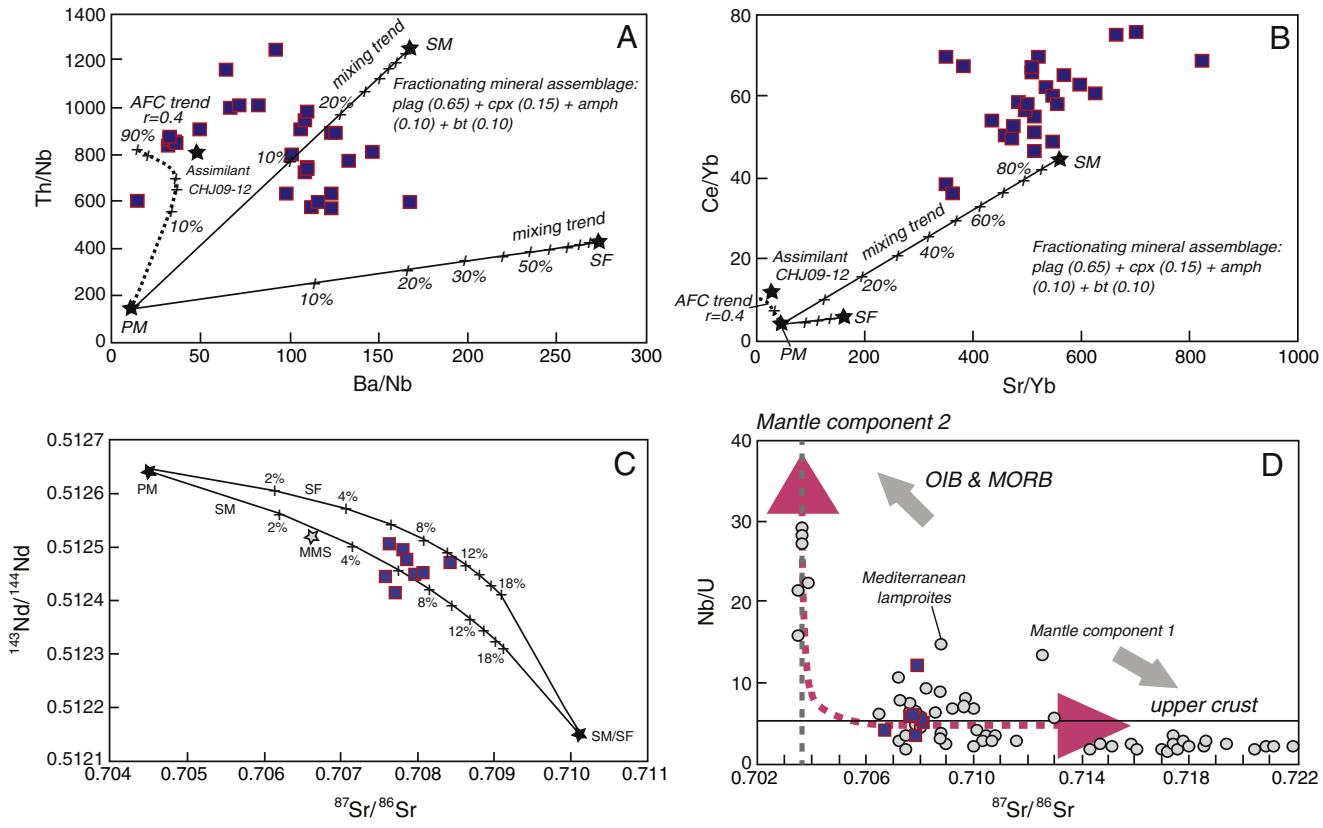

Fig. 14. (A and B) Th/Nb vs. Ba/Nb and Ce/Yb vs. Sr/Yb diagrams to evaluate the effect of sediment fluids and sediment-derived melts on the mantle wedge (primary mantle; PM) source (mixing trends). For comparison we have also added the AFC trend like as that described in Fig. 13. The geochemical composition of sediment melts (SM), sediment fluid (SF) and primary mantle (PM) are reported in Table 4; (C) $^{143}Nd/^{144}Nd$ vs. $^{87}Sr/^{86}Sr$ diagram showing the mixing trend between the primary mantle (PM), sediment melt (SM) and fluid (SF) compositions. The compositions of primary mantle (PM), Mixed Mantle Source (MMS), sediment melts (SM) and fluids (SF) are from Ersoy et al. (2010) and reported in Table 4; (D) Identification of mantle components of the Saray volcanic rocks using Nb/U vs. $^{87}Sr/^{86}Sr$ ratios.
Modified after Prelević et al. (2012).

Quaternary period (e.g., Didon and Germain, 1976; Dostal and Zebri, 1978). This temporal shift from a lithospheric to an asthenospheric source is correlated to asthenospheric upwelling through a tear on the subducted slab of the Arabian plate (Prelević et al., 2012).

7. Conclusions

The Saray high-K rocks in NW Iran yield Ar–Ar ages of ~11 Ma (Late Miocene) and comprise 1) tephritic, phonolitic, trachytic and leucititic lavas, 2) huge volumes of pyroclastic rocks and 3) trachytic, basanitic and lamproitic dikes crosscutting the above rock units. These rocks are highly enriched in incompatible trace elements and have highly radiogenic Sr and Pb isotopes with non-radiogenic Nd isotopes. The rocks contain clinopyroxene phenocrysts with complex zoning including Al–Ti rich and/or Al–Ti poor varieties. The geochemical features and modeling results indicate that these rocks were produced by the partial melting of refertilized and metasomatized mantle sources with less effect of crystal fractionation, but dominated by AFC processes. Isotopically, the Saray volcanic rocks define a binary mixing trend, representing 5–8%mixing between the primary mantle (PM) and sediment melts. Melting of subducted sediments could have supplied the required crustal components to the mantle source of the Saray volcanic rocks. Continental collision between Arabia and Eurasia led to slab-break-off and the development of an asthenospheric window, facilitating partial melting of the subduction-contaminated sub-continental lithospheric mantle, resulting in the formation of the high-K rocks.

The geochemical features suggest an enriched mantle source as the dominant component for the leucite-bearing rocks, phonolites, and basanites. In the more fractionated trachytes, some crustal contamination is indicated. The enrichment of the mantle source could have occurred during late Proterozoic or early Paleozoic — or during a relatively recent event, but involved fluids that interacted with the older rocks. The starting mantle material was probably subcontinental mantle that was isolated from the asthenospheric mantle mixing at the time of initial crust stabilization. Subsequently, the subcontinental mantle was enriched by subduction-related fluids or melts. Finally, the enriched mantle underwent low degrees of melting (probably ~2–10%) resulting in the production of high-K rocks. Some of these melts interacted with the crust during their ascent to the surface, resulting in the incorporation of crustal components.

Supplementary data to this article can be found online at http://dx.doi.org/10.1016/j.gr.2013.09.015.

Acknowledgments

We thank Prof. Zeming Zhang for his efficient editorial handling and two anonymous referees for their helpful comments which enhanced the scientific value of this paper. Partial support from Damghan University (Iran) is acknowledged. The first author (HSM) thanks Y. Ersoy for providing him the latest version of FC–AFC–FCA and mixing modeler software. Special thanks go to M.A. Gracía for the assistance during mass spectrometry and A.S. Rosas Montoya and V.M. Pérez Arroyo for the sample preparation during the Ar–Ar dating. Sh. Shahabi is thanked for the assistance during the field work. We thank also S. Moghadasi and A. Torabi for their help during the thin section and

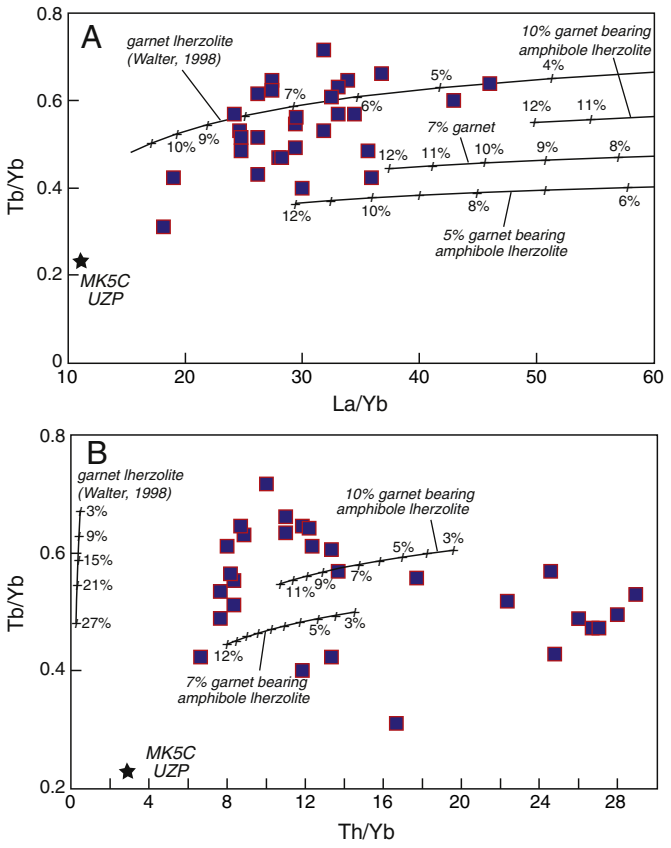

Fig. 15. Trace element non-modal dynamic melting models (with critical melt porosity of 1.1%) of the Saray lavas for garnet bearing amphibole lherzolites from Ulten Zone (Sample MK5C; Rampone and Morten, 2001) with varying amount of garnet (5, 7 and 10%) (See Table 5 for source composition and melting mode). For comparison the melting trend of garnet lherzolite composition of Walter (1998) is shown (See Table 5 for composition and melt mode).

Table 5
The composition and melting mode of the garnet lherzolite (Walter, 1998) and Ulten Zone (UZP) (Rampone and Morten, 2001) mantle sources.

	Garnet–lherzolite (Walter, 1998)	UZP (sample MK5C) 7% garnet	UZP (sample MK5C) 5% garnet	UZP (sample MK5C) 3% garnet	UZP (sample MK5C) 10% garnet
Source mode					
Olivine	57.0%	54.0%	54.0%	54.0%	54.0%
Opx	21.0%	21.0%	21.0%	21.0%	20.0%
Cpx	16.0%	12.0%	14.0%	15.0%	10.0%
Garnet	6.0%	7.0%	5.0%	3.0%	10.0%
Amphibole	0.0%	6.0%	6.0%	6.0%	6.0%
Melt mode					
Olivine	8.0%	5.0%	5.0%	5.0%	5.0%
Opx	−19.0%	5.0%	5.0%	5.0%	5.0%
Cpx	81.0%	30.0%	30.0%	30.0%	30.0%
Garnet	30.0%	20.0%	20.0%	20.0%	20.0%
Amphibole	0.0%	40.0%	40.0%	40.0%	40.0%

Trace elements composition of the Ulten Zone Peridotites (Eastern Italian Alps)	
Th	0.620
La	2.420
Tb	0.050
Yb	0.220

Trace elements composition of garnet lherzolite of Walter (1998)	
Th	0.029
La	1.651
Tb	0.069
Yb	0.269

microphotograph preparations. This study also contributes to the 1000 Talent Award from the Chinese Government to M. Santosh.

References

Adamia, S.A., Lordkipanidze, M.B., Zakariadze, G.S., 1977. Evolution of an active continental margin as exemplified by the Alpine history of the Caucasus. Tectonophysics 40, 183–189.

Agard, P., Omrani, J., Jolivet, L., Mouthereau, F., 2005. Convergence history across Zagros (Iran): constraints from collisional and earlier deformation. International Journal of Earth Sciences 94, 401–419.

Aldanmaz, E., Pearce, J.A., Thirlwall, M.F., Mitchell, J.G., 2000. Petrogenetic evolution of Late Cenozoic, post-collision volcanism in western Anatolia, Turkey. Journal of Volcanology and Geothermal Research 102, 67–95.

Aldanmaz, E., Köprübaşı, N., Gürer, O.F., Kaymakcı, N., Gourgaud, A., 2006. Geochemical constraints on the Cenozoic, OIB-type alkaline volcanic rocks of NW Turkey: implications for mantle sources and melting processes. Lithos 86, 50–76.

Alici Sen, P., Temel, A., Gourgaud, A., Kieffer, G., Gundogdu, M.N., 2004. Petrology and geochemistry of potassic rocks in the Golcuk area (Isparta, SW Turkey): genesis of enriched alkaline magmas. Journal of Volcanology and Geothermal Research 85, 423–446.

Allen, B.M., Vincent, S.J., Ismail-zadeh, A., Simmons, M., Anderson, L., 2002. Onset of subduction as the cause of rapid Pliocene–Quaternary subsidence in the South Caspian basin. Geology 30, 775–778.

Allen, M.B., Kheirkhah, M., Nill, I., Emami, M.H., Mcleod, C., 2013. Generation of arc and within-plate chemical signatures in collision zone magmatism: Quaternary lavas from Kurdistan province, Iran. Journal of Petrology 54, 887–911.

Altunkaynak, Ş., Genç, C., 2008. Petrogenesis and time-progressive evolution of the Cenozoic continental volcanism in the Biga Peninsula, NW Anatolia (Turkey). Lithos 102, 316–340.

Altunkaynak, S., Diley, Y., Genc, C.S., Sunal, G., Gertisser, R., Furnes, H., Foland, K.A., Yang, J., 2012. Spatial, temporal and geochemical evolution of Oligo–Miocene granitoid magmatism in western Anatolia, Turkey. Gondwana Research 21, 961–986.

Bektaş, O., Şen, C., Atıcı, Y., Köprübaşı, N., 1999. Migration of the Upper Cretaceous subduction-related volcanism toward the back-arc basin of the eastern Pontide magmatic arc (NE Turkey). Geological Journal 34, 95–106.

Bell, K., Castorina, F., Lavecchia, G., Rosatelli, G., Stoppa, F., 2004. Is there a mantle plume below Italy? EOS. Transactions of the American Geophysical Union 85, 541–547.

Bell, K., Lavecchia, G., Rosatelli, G., 2013. Cenozoic Italian magmatism — isotope constraints for possible plume-related activity. Journal of South American Earth Sciences 41, 22–40. Berberian, M., King, G.C.P., 1981. Towards a paleogeography and tectonic evolution of Iran. Canadian Journal of Earth Sciences 18, 210–265.

Beydoun, Z.R., Hughes Clarke, M.W., Stoneley, R., 1992. Petroleum in the Zagros basin: a Late Tertiary foreland basin overprinted onto the outer edge of a vast hydrocarbon-rich Palaeozoic–Mesozoic passive margin shelf. Association of Petroleum Geologists, Memoir 55, 309–339.

Bianchini, G., Yoshikawa, M., Sapienza, G.T., 2010. Comparative study of ultramafic xenoliths and associated lavas from South-Eastern Sicily: nature of the lithospheric mantle and insights on magma genesis. Mineralogy and Petrology 98, 111–121. Buddington, A.F., Lindsley, D.H., 1964. Iron–titanium oxide minerals and synthetic equivalents. Journal of Petrology 5, 310–357.

Carpentier, M., Chauvel, C., Maury, R.C., Mattielli, N., 2009. The 'zircon effect' as recorded by the chemical and Hf isotopic compositions of Lesser Antilles forearc sediments. Earth and Planetary Science Letters 287, 86–99.

Castillo, P.R., Janney, P.E., Solidum, R., 1999. Petrology and geochemistry of Camiguin Island, southern Philippines: insights into the source of adakite and other lavas in a complex arc tectonic setting. Contributions to Mineralogy and Petrology 134, 33–51.

Cellai, D., Conticelli, S., Menchetti, S., 1994. Crystal-chemistry of clinopyroxenes in Italian lamproites and kamafugites: implications on their genesis. Contributions to Mineralogy and Petrology 116, 301–315.

Chiu, H., Chung, S., Zarrinkoub, M., Mohammadi, S., Khatib, M., Iizuka, Y., 2013. Zircon U–Pb age constraints from Iran on the magmatic evolution related to Neotethyan subduction and Zagros orogeny. Lithos 162–163, 70–87.

Chorowicz, J., Dhont, D., Adıyaman, Ö., 1998. Black Sea–Pontid relationship: interpretation in terms of subduction. Third International Turkish Geology Symposium: Ankara, Turkey, p. 258 (Abstracts).

Conceição, R.V., Green, D.H., 2004. Derivation of potassic (shoshonitic) magmas by decompressing melting of phlogopite + pargasite lherzolite. Lithos 72, 209–229.

Conticelli, S., Peccerillo, A., 1990. Petrological significance of high-pressure ultramafic xenoliths from ultrapotassic rocks of Central Italy. Lithos 24, 305–322.

Conticelli, S., Peccerillo, A., 1992. Petrology and geochemistry of potassic and ultrapotassic volcanism in central Italy: petrogenesis and inferences on the evolution of the mantle sources. Lithos 28, 221–240.

Conticelli, S., Manetti, P., Menichetti, S., 1992. Petrology, chemistry, mineralogy and Sr-isotopic features of Pliocenic orendites from South Tuscany: implications on their genesis and evolutions. European Journal of Mineralogy 4, 1359–1375.

Conticelli, S., Francalanci, L., Manetti, P., Cioni, R., Sbrana, A., 1997. Petrology and geochemistry of the ultrapotassic rocks from the Sabatini Volcanic District, Central Italy: the role of evolution-ary processes in the genesis of variably enriched alkaline magmas. Journal of Volcanology and Geothermal Research 75, 107–136.

Conticelli, S., Guarnieri, L., Farinelli, A., Mattei, M., Avanzinelli, R., Bianchini, G., Boari, E., Tommasini, S., Tiepolo, M., Prelevic, D., Venturelli, G., 2009. Trace elements and Sr–Nd–Pb isotopes of K-rich, shoshonitic, and calc-alkaline magmatism of the western Mediterranean region: genesis of ultrapotassic to calc alkaline magmatic associations in a post-collisional geodynamic setting. Lithos 107, 68–92.

Conticelli, S., Avanzinelli, R., Marchionni, S., Tommasini, S., Melluso, L., 2011. Sr–Nd–Pb isotopes from the Radicofani Volcano, Central Italy: constraints on heterogeneities in a veined mantle responsible for the shift from ultrapotassic shoshonite to basaltic andes-ite magmas in a post-collisional setting. Mineralogy and Petrology 103, 123–148.

Conticelli, S., Avanzinelli, R., Poli, G., Braschi, E., Giordano, G., 2012. Shift from lamproite-like to leucititic rocks: Sr–Nd–Pb isotope data from the Monte Cimino volcanic complex vs. the Vico stratovolcano, Central Italy. Chemical Geology. http://dx.doi.org/10.1016/j.chemgeo.2012.10.018.

Defant, M., Drummond, M., 1990. Derivation of some modern arc magmas by melting of young subducted lithosphere. Nature 347, 662–665.

Defant, M., Drummond, M., 1993. Mount Street Helens: potential example of the partial melting of the subducted lithosphere in a volcanic arc. Geology 21, 547–550. DePaolo, D.J., 1981. Trace element and isotopic effects of combined wallrock assimilation and fractional crystallization. Earth and Planetary Science Letters 53, 189–202. Dercourt, J., Zonenshain, L.P., Ricou, L.-E., Kazmin, V.G., Le Pichon, X., Knipper, A.L., Grandjacquet, C., Sbortshikov, I.M., Geyssant, J., Lepvrier, C., Pechersky, D.H., Boulin, J., Sibuet, J.-C., Savostin, L.A., Sorokhtin, O., Westphal, M., Bazhenov, M.L., Lauer, J.P., Biju-Duval, B., 1986. Geological evolution of the Tethys belt from the Atlantic to the Pamirs since the Lias. Tectonophysics 123, 241–315.

Dewey, J.F., Pitman, W.C., Ryan, W.B.F., Bonnin, J., 1973. Plate tectonics and evolution of the Alpine system. Geological Society of America Bulletin 84, 3137–3180.

Didon, J., Germain, Y.M., 1976. Le Sabalan, Volcan Plio–Quaternaire de l'Azerbaidjan oriental (Iran). (These) Etude geologique et petrographique de le difice et de son environment regional.Docteur du 3 eme cycle. Univ. Grenoble, France (304 pp.).

Dilek, Y., Altunkaynak, S., 2009. Geochemical and temporal evolution of Cenozoic magmatism in western Turkey: mantle response to collision, slab breakoff, and lithospheric tearing in an orogenic belt. In: van Hinsbergen, D.J.J., Edwards, M.A., Govers, R. (Eds.), Geodynamics of Collision and Collapse at the Africa–Arabia–Eurasia Subduction Zone. Geological Society of London Special Publication, pp. 213–234.

Dilek, Y., Imamverdiyev, N., Altunkaynak, S., 2010. Geochemistry and tectonics of Cenozoic volcanism in the Lesser Caucasus (Azerbaijan) and the peri-Arabian region: collision-induced mantle dynamics and its magmatic fingerprint. International Geology Review 52, 536–578.

Dokuz, A., 2011. A slab detachment and delamination model for the generation of Carboniferous high-potassium I-type magmatism in the Eastern Pontides, NE Turkey: the Kose composite pluton. Gondwana Research 19, 926–944.

Dostal, J., Zebri, M., 1978. Geochemistry of Savalan volcano (northwestern Iran). Chemical Geology 22, 31–42.

Elitok, O., Ozgur, N., Druppel, K., Dilek, Y., Platevoet, B., Guillou, H., Poisson, A., Scaillet, S., Satir, M., Siebel, W., Bardintzeff, J.M., Deniel, H., Yilmaz, K., 2010. Origin and geodynamic evolution of late Cenozoic potassium-rich volcanism in the Isparta area, southwestern Turkey. International Geology Review 52, 454–504.

Ersoy, E.Y., Helvacı, C., 2010. FC–AFC–FCA and mixing modeler: a Microsoft Excel spreadsheet program for modeling geochemical differentiation of magma by crystal fractionation, crustal assimilation and mixing. Computers and Geosciences 36, 383–390.

Ersoy, E.Y., Helvacı, C., Sözbilir, H., Erkül, F., Bozkurt, E., 2008. A geochemical approach to Neogene–Quaternary volcanic activity of western Anatolia: an example of episodic bimodal volcanism within the Selendi Basin, Turkey. Chemical Geology 255, 265–282.

Ersoy, E.Y., Helvacı, C., Palmer, M.R., 2010. Mantle source characteristics and melting models for the early-middle Miocene mafic volcanism in Western Anatolia: implications for enrichment processes of mantle lithosphere and origin of K-rich volcanism in post-collisional settings. Journal of Volcanology and Geothermal Research 198, 112–128.

Ersoy, E.Y., Helvacı, C., Uysal, I., Karaoğlu, O., Palmer, M.R., Dindi, F., 2012a. Petrogenesis of the Miocene volcanism along thelzmir–Balıkesir Transfer Zone in western Anatolia, Turkey: implications for origin and evolution of potassic volcanism in post-collisional areas. Journal of Volcanology and Geothermal Research 241–242, 21–38.

Ersoy, E.Y., Helvacı, C., Palmer, M.R., 2012b. Petrogenesis of the Neogene volcanic units in the NE–SW-trending basins in western Anatolia, Turkey. Contributions to Mineralogy and Petrology 163, 379–401.

Eyuboglu, Y., 2010. Late Cretaceous high-K volcanism in the eastern Pontides orogenic belt, and its implications for the geodynamic evolution of NE Turkey. International Geology Review 52, 142–186.

Eyuboglu, Y., 2013. Slab window magmatism and convergent margin tectonics. Geoscience Frontiers 4, 349–351.

Eyuboglu, Y., Bektaş, O., Seren, A., Maden, N., Jacoby, W.R., Özer, R., 2006. Three axial extensional deformation and formation of the Liassic rift basins in the Eastern Pontides (NE Turkey). Geologica Carpathica 57, 337–346.

Eyuboglu, Y., Bektaş, O., Pul, D., 2007. Mid-Cretaceous olistostromal ophiolitic melange developed in the back-arc basin of the eastern Pontide magmatic arc (NE Turkey). International Geology Review 49, 1103–1126.

Eyuboglu, Y., Dilek, Y., Bozkurt, E., Bektaş, O., Rojay, B., Şen, C., 2010. Geochemistry and geochronology of a reversely-zoned, Alaskan-type ultramafic–mafic complex in the Eastern Pontides, NE Turkey. In: Santosh, M., Maruyama, S. (Eds.), A Tribute to Akiho Miyashiro. Gondwana Research, 18, pp. 230–252.

Eyuboglu, Y., Chung, S.L., Santosh, M., Dudas, F.O., Akaryali, E., 2011a. Transition from shoshonitic to adakitic magmatism in the Eastern Pontides, NE Turkey: implications for slab window melting. Gondwana Research 19, 413–429.

Eyuboglu, Y., Santosh, M., Dudas, F.O., Chung, S.L., Akaryali, E., 2011b. Migrating magmatism in a continental arc: geodynamics of the Eastern Mediterranean revisited. Journal of Geodynamics 52, 2–15.

Eyuboglu, Y., Santosh, M., Chung, S.L., 2011c. Crystal fractionation of adakitic magmas in the crust-mantle transition zone: petrology, geochemistry and U–Pb zircon chronology of the Seme adakites, Eastern Pontides, NE Turkey. Lithos 121, 151–166. Eyuboglu, Y., Santosh, M., Bektaş, O., Ayhan, S., 2011d. Arc magmatism as a window to plate kinematics and subduction polarity: example from the Eastern Pontides belt, NE Turkey. Geoscience Frontiers 2, 49–56.

Eyuboglu, Y., Santosh, M., Chung, S.L., 2011e. Petrochemistry and U–Pb ages of adakitic intrusions from the Pulur massif (Eastern Pontides, NE Turkey): implications for slab roll-back and ridge subduction associated with Cenozoic convergent tectonics in eastern Mediterranean. Journal of Geology 119, 394–417.

Eyuboglu, Y., Santosh, M., Yi, K., Bektaş, O., Kwon, S., 2012. Discovery of Miocene adakitic dacite from the Eastern Pontides Belt and revised geodynamic model for the late Cenozoic Evolution of eastern Mediterranean region. Lithos 146–147, 218–232. Eyuboglu, Y., Santosh, M., Dudas, F.O., Akaryali, E., Chung, S.L., Akdag, K., Bektas, O., 2013a. The nature of transition from adakitic to non-adakitic magmatism in a slab-window setting: a synthesis from the eastern Pontides, NE Turkey. Geoscience Frontiers 4, 353–375.

Eyuboglu, Y., Dudas, F.O., Santosh, M., Yi, K., Kwon, S., Akaryalı, E., 2013b. Petrogenesis and U–Pb zircon chronology of adakitic porphyries within the Kop ultramafic massif (Eastern Pontides Orogenic Belt, NE Turkey). Gondwana Research. http://dx.doi.org/ 10.1016/j.gr.2012.11.014.

Farley, K.A., Natland, J.H., Craig, H., 1992. Binary mixing of enriched and undegassed (primitive?) mantle components (He, Sr, Nd, Pb) in Samoan lavas. Earth and Planetary Science Letters 111, 183–199.

Foley, S.F., 1992. Vein-plus-wall-rock melting mechanisms in the lithosphere and the origin of potassic alkaline magmas. Lithos 28, 435–453.

Foley, S.F., Venturelli, G., Green, D.H., Toscani, L., 1987. The ultrapotassic rocks: characteristics, classification and constraints for petrogenetic models. Earth Science Reviews 24, 81–134.

Frezzotti, M., Angelo Peccerillo, A., Panza, G., 2009. Carbonate metasomatism and CO2 lithosphere–asthenosphere degassing beneath the Western Mediterranean: An integrated model arising from petrological and geophysical data. Chemical Geology 262, 108–120.

Gasparon, M., Varne, R., 1998. Crustal assimilation versus subducted sediment input in west Sunda arc volcanics: an evaluation. Mineralogy and Petrology 64, 89–117. Gregoire, M., Bell, D.R., Roux, A.P.L., 2002. Trace element geochemistry of phlogopite-rich mafic mantle xenoliths: their classification and their relationship to phlogopite-bearing peridotites and kimberlites revisited. Contributions to Mineralogy and Petrology 142, 603–625.

Gulec, N., 1991. Crust–mantle interaction in western Turkey: implications from Sr and isotope geochemistry of Tertiary and Quaternary volcanics. Geological Magazine 128, 417–435.

Handely, H.K., Turner, S., Macpherson, C.G., Gertisser, R., Davidson, J.P., 2011. Hf–Nd isotope and trace element constraints on subduction inputs at island arcs: limitations of Hf anomalies as sediment input indicators. Earth and Planetary Science Letters 304, 212–223.

Hart, S.R., 1984. A large-scale isotope anomaly in the Southern Hemisphere mantle. Nature 309, 753–757.

Hart, S.R., Hauri, E.H., Oschmann, L.A., Whitehead, J.A., 1992. Mantle plumes and entrainment: isotopic evidence. Science 256, 517–520.

Hartmann, G., Wedepohl, K.H., 1993. The composition of peridotite tectonites from the Ivrea Complex, Northern Italyç residues from melt extraction. Geochimica et Cosmochimica Acta 57, 1761–1782.

Hassanzadeh, J., Stockli, D.F., Horton, B.K., Axen, G.J., Stockli, L.D., Grove, M., Schmitt, A.K., Walker, J.D., 2008. U–Pb zircon geochronology of late Neoproterozoic–Early Cambrian granitoids in Iran: implications for paleogeography, magmatism, and exhumation history of Iranian basement. Tectonophysics 451, 71–96.

Hawkesworth, C.J., Hergt, J.M., Ellam, R.M., McDermott, P., 1991. Element fluxes associated with subduction related magmatism. Philosophical Transactions of the Royal Society of London A 335, 393–405.

Hawkesworth, C.J., Turner, S.P., McDermott, F., Peate, D.W., Van Calsteren, P., 1997. U–Th isotopes in Arc magmas: implications for element transfer from the subducted crust. Science 276, 551–555.

Hempton, M.R., 1987. Constraints on Arabian plate motion and extensional history of the Red Sea. Tectonics 6, 687–705.

Hofmann, A.W., Jochum, K.P., 1996. Source characteristics derived from very incompatible trace elements in Mauna Loa and Mauna Kea basalts, Hawaii Scientific Drilling Project. Journal of Geophysical Research B: Solid Earth and Planets 101, 11831–11839. Jahangiri, A., 2007. Post-collisional Miocene adakitic volcanism in NW Iran: geochemical and geodynamic implications. Journal of Asian Earth Sciences 30, 433–447.

Kelemen, P.B., MacLeod, C., Umino, S. (Eds.), 2004. The Oman Ophiolite and Mid-Ocean Ridge Processes. G3. AGU Publication.

Keskin, M., 2003. Magma generation by slab steepening and breakoff beneath a subduction–accretion complex: an alternative model for collision-related volcanism in Eastern Anatolia, Turkey. Geophysical Research Letters 30 (24), 8046. http://dx.doi.org/10.1029/2003GL018019.

Keskin, M., Pearce, J.A., Mitchell, J.G., 1998. Volcano-stratigraphy and geochemistry of collision-related volcanism on the Erzurum–Kars Plateau, northeastern Turkey. Journal of Volcanology and Geothermal Research 85, 355–404.

Khedr, M.Z., Arai, S., Tamura, A., Morishita, T., 2010. Clinopyroxenes in high-P metaperidotites from Happo-O'ne, central Japan: implications for wedge-transversal chemical change of slab-derived fluids. Lithos 119, 439–456.

Kheirkhah, M., Allen, M., Emami, M., 2009. Quaternary syn-collision magmatism from the Iran–Turkey borderlands. Journal of Volcanology and Geothermal Research 182, 1–12. Le Bas, M.J., Le Maitre, R.W., Streckeisen, A., Zanettin, B., 1986. A chemical classification of volcanic rocks based on the total alkali–silica diagram. Journal of Petrology 27, 745–750.

Lu, Y.J., Kerrich, R., Cawood, P.A., McCuaig, T.C., Hart, C.J.R., Li, Z.X., Hou, Z.Q., Bagas, L., 2012. Zircon SHRIMP U–Pb geochronology of potassic felsic intrusions in western Yunnan, SW China: constraints on the relationship of magmatism to the Jinsha suture. Gondwana Research 22, 737–747.

Maden, N., 2013. Geothermal structure of the eastern Black Sea basin and eastern Pontides orogenic belt: implications for subduction polarity of Tethys oceanic lithosphere. Geoscience Frontiers. http://dx.doi.org/10.1016/j.gsf.2013.02.001. McCulloch, M.T., Gamble, A.J., 1991. Geochemical and geodynamical constraints on subduction zone magmatism. Earth and Planetary Science Letters 102, 358–374.

Mitchell, R.H., Bergman, S.E., 1991. Petrology of Lamproites. Plenum, New York (447 pp.). Mitchell, R.H., Smith, C.B., Vladykin, N.V., 1994. Isotopic composition of strontium and neodymium in potassic rocks of the Little Murun complex, Aldan Shield, Siberia. Lithos 32, 243–248.

Moine-Vaziri, H., Khalili Marandi, S.H., Brousse, R., 1991. Importance doun volcanism potassique, au Miocene Superier, en Azerbaijan, Iran. Comptes Rendus de l'Académie des Sciences, Paris 313, 1603–1610.

Morimoto, N., Fabries, J., Ferguson, A.K., Ginzburg, I.V., Ross, M., Seifert, F.A., Zussman, J., Aoki, K., Gottardi, G., 1998. Nomenclature of pyroxenes. Mineralogical Magazine 52, 535–550. Muller, B., Zoback, M.L., Fuchs, K., Mastin, L., Gregersen, S., Pavoni, N., Stephanson, O., Ljunggren, C.H., 1992. Regional patterns of tectonic stress in Europe. Journal Geophysical Research 97 (B8), 11 783–11 803.

Nelson, S.T., Montana, A., 1992. Sieve-textured plagioclase in volcanic rocks produced by rapid decompression. American Mineralogist 77, 1242–1249.

Okay, A.I., Sahintürk, Ö., 1997. Geology of the Eastern Pontides. In: Robinson, A.G. (Ed.), Regional and Petroleum Geology of the Black Sea and Surrounding Region. American Association of Petroleum Geologists Memoir, 68, pp. 291–311.

Omrani, J., Agard, P., Whitechurch, H., Benoit, M., Prouteau, G., Jolivet, L., 2008. Arc-magmatism and subduction history beneath the Zagros Mountains Iran. A new report of adakites and geodynamic consequences. Lithos 106, 380–398.

Pang, K.N., Chung, S.L., Zarrinkoub, H.S., Lin, Y.C., Lee, H.Y., Lo, C.H., Khatib, M.M., 2013. Iranian ultrapotassic volcanism at ~11 Ma signifies the initiation of postcollisional magmatism in the Arabia–Eurasia collision zone. Terra Nova 25 (5), 405–413. Pearce, J.A., 1982. Trace element characteristics of lavas from destructive plate boundaries. In: Thorpe, R.S. (Ed.), Andesites. Wiley, New York, pp. 525–548.

Pearce, J.A., Cann, J.R., 1973. Tectonic setting of basic volcanic rocks determined using trace element analyses. Earth and Planetary Science Letters 19, 290–300.

Pearce, J.A., Parkinson, I.J., 1993. Trace element models for mantle melting: application to volcanic arc petrogenesis. In: Prichard, H.M., Alabaster, T., Harris, N.B.W., Neary, C.R.(Eds.), Magmatic Processes and Plate Tectonics. Geological Society of London Special Publication, 76, pp. 373–403.

Pearce, J.A., Peate, D.W., 1995. Tectonic implications of the composition of volcanic arc magmas. Annual Review of Earth and Planetary Sciences 23, 251–285.

Pearce, J.A., Bender, J.F., De Long, S.E., Kidd, W.S.F., Low, P.J., Guner, Y., Saroglu, F., Yilmaz, Y., Moorbath, S., Mitchell, J.G., 1990. Genesis of collision volcanism in Eastern Anatolia, Turkey. Journal of Volcanology and Geothermal Research 44, 189–229. Peccerillo, A., Taylor, S.R., 1976. Geochemistry of Eocene calc-alkaline volcanic rocks from Kastamonu area, Northern Turkey. Contributions to Mineralogy and Petrology 58, 63–81.

Pe-Piper, G., Piper, D.J.W., Koukouvelas, I., Dolansky, L., Kokkalas, S., 2009. Postorogenic shoshonitic rocks and their origin by melting underplated basalts: The Miocene of Limnos, Greece. Geological Society of America Bulletin 121, 39–54.

Perini, G., Francalanci, L., Davidson, J.P., Conticelli, S., 2004. The petrogenesis of Vico Volcano, Central Italy: an example of low scale mantle heterogeneity. Journal of Petrology 45, 139–182.

Plank, T., Langmuir, C.H., 1998. The chemical composition of subducting sediments and its consequence for the crust and mantle. Chemical Geology 145, 325–394.

Prelević, D., Foley, S.F., 2007. Accretion of arc-oceanic lithospheric mantle in the Mediterranean: evidence from extremely high-Mg olivines and Cr-rich spinel inclusions from lamproites. Earth and Planetary Science Letters 256, 120–135.

Prelević, D., Foley, S.F., Cvetković, V., Romer, R.L., 2004. Origin of minette by mixing of lamproite and dacite magmas in Veliki Majdan Serbia. Journal of Petrology 45, 759–792.

Prelević, D., Foley, S.F., Cvetković, V., Romer, R.L., Downes, H., 2005. Tertiary ultrapotassic volcanism in Serbia: constraints on petrogenesis and mantle source characteristics. Journal of Petrology 46, 1443–1487.

Prelević, D., Foley, S.F., Romer, R.L., Conticelli, S., 2008. Mediterranean Tertiary lamproites: multicomponent melts in post-collisional geodynamics. Geochimica et Cosmochimica Acta 72, 2125–2156.

Prelević, D., Akal, C., Foley, S., Romer, R., Stracke, A., Van Den Bogaard, P., 2012. Ultrapotassic mafic rocks as geochemical proxies for post-collisional dynamics of orogenic lithospheric mantle: the case of southwestern Anatolia, Turkey. Journal of Petrology 53, 1019–1055.

Rampone, E., Morten, L., 2001. Records of crustal metasomatism in the garnet peridotites of the Ulten Zone (Upper Austroalpine, Eastern Alps). Journal of Petrology 42, 207–219. Rock, N.M.S., 1987. Nature and origin of calc-alkaline lamprophyres: a review. In: Fitton, J.G., Upton, B.G.J. (Eds.), Alkaline Igneous Rocks. Geological Society Special Publication, 30, pp. 191–226.

Sapienza, G.T., Scambelluri, M., Braga, R., 2009. Dolomite-bearing orogenic garnet peridotites witness fluid-mediated carbon recycling in a mantle wedge (Ulten Zone, Eastern Alps, Italy). Contributions to Mineralogy and Petrology. http://dx.doi.org/10.1007/s00410-009-0389-2.

Schreyer, W., Massonne, H.J., Chopin, C., 1987. Continental crust subducted to depths near 100 km; implications for magma and fluid genesis in collision zones. In: Mysen, B.O. (Ed.), Magmatic processes; Physicochemical Principles; A Volume in Honor of Hatten S. Yoder, Jr. Special Publication, 1. Geochemical Society, St Louis (Mo.), pp. 155–163.

Sengor, A.M.C., Natalin, B.A., 1996. Paleotectonics of Asia: fragments of a synthesis. In: Yin, A., Harrison, T.M. (Eds.), The Tectonic Evolution of Asia. Cambridge University Press, pp. 486–640.

Sengor, A.M.C., Yılmaz, Y., 1981. Tethyan evolution of Turkey: a plate tectonic approach. Tectonophysics 75, 181–241.

Shafaii Moghadam, H., Stern, R.J., 2011. Geodynamic evolution of Upper Cretaceous Zagros ophiolites: formation of oceanic lithosphere above a nascent subduction zone. Geological Magazine 148, 762–801.

Shafaii Moghadam, H., Stern, R.J., Kimura, J.I., Hirahara, Y., Senda, R., Miyazaki, T., 2012. Hf–Nd isotope constraints on the origin of Dehshir Ophiolite, Central Iran. The Island Arc 21, 202–214.

Shafaii Moghadam, H., Khademi, M., Hu, Z., Stern, R.J., Santos, J.F., Wu, Y., 2013. Cadomian (Ediacaran-Cambrian) arc magmatism in the ChahJam-Biarjmand metamorphic complex (Iran): magmatism along the northern active margin of Gondwana. Gondwana Reserach (paper revised).

Shahabi, Sh., 2013. Geochemistry, Petrology and Dating of Alkaline Granites (A-type) and Gabbros of Ghoshchi Region (NW Iran). (Msc. Thesis) Damghan University (120 pp.). Sorensen, H., Bernth, U., Brousse, R., 1999. Trachytes and phonolites from the Mont–Dore region, Auvergne, France. Geolines 9, 114–118.

Temel, A., Gundogdu, M.N., Gourgaud, A., 1998. Petrological and geochemical characteristics of Cenozoic high-K calc-alkaline volcanism in Konya, Central Anatolia, Turkey. Journal of Volcanology and Geothermal Research 85, 327–354.

Tommasini, S., Avanzinelli, R., Conticelli, S., 2011. The Th/La and Sm/La conundrum of the Tethyan realm lamproites. Earth and Planetary Science Letters 301, 469–478.

Tsuchiyama, A., 1985. Dissolution kinetics of plagioclase in the melt system diopside–albite–anorthite, and origin of dusty plagioclase in andesites. Contributions to Mineralogy and Petrology 89, 1–16.

Turner, S., Hawkesworth, C., Gallagher, K., Stewart, K., Peate, D., Mantovani, M., 1996. Mantle plumes, flood basalts, and thermal models for melt generation beneath continents: assessment of a conductive heating model and application to the Paran. Journal of Geophysical Research 101, 11503–11518.

Walter, M.J., 1998. Melting of garnet peridotite and the origin of komatiite and depleted lithosphere. Journal of Petrology 39, 29–60.

Workman, R.K., Hart, S.R., Jackson, M., Regelous, M., Farley, K.A., Blusztajin, J., Kurz, M., Staudigel, H., 2004. Recycled metasomatized lithosphere as the origin of the enriched mantle II (EM2) end-member: evidence from the Samoan Volcanic Chain. Geochemistry, Geophysics, Geosystems. http://dx.doi.org/10.1029/2003GC000623.

Yilmaz, Y., Guner, Y., Saroglu, F., 1998. Geology of the Quaternary volcanic centers of East Anatolia. Journal of Volcanology and Geothermal Research 85, 173–210.

Yılmaz, Y., Tüysüz, O., Yiğitbaş, E., Genç, Ş.C., Şengör, A.M.C., 1997. Geology and tectonic evolution of the Pontides. In: Robınson, A.G. (Ed.), Regional and Petroleum Geology of the Black Sea and Surrounding Region. AAPG Memoir, 68, p. 183226.

Yılmaz, Y., Genç, Ş.C., Karacik, Z., Altunkaynak, S., 2001. Two contrasting magmatic associations of NW Anatolia and their tectonic significance. Journal of Geodynamics 31, 243–271.

Zhang, R.Y., Pan, Y.M., Yang, Y.H., Li, T.F., Liou, J.G., Yang, J.S., 2008. Chemical composition and ultrahigh-P metamorphism of garnet peridotites from the Sulu UHP terrane, China: investigation of major, trace elements and Hf isotopes of minerals. Chemical Geology 255 (1–2), 250–264.

Zhao, Z.D., Mo, X.X., Dilek, Y., Niu, Y.L., DePaolo, D.J., Robinson, P., Zhu, D.C., Sun, C.G., Dong, G.C., Zhou, S., Luo, Z.H., Hou, Z.Q., 2009. Geochemical and Sr–Nd–Pb–O isotopic compositions of the post-collisional ultrapotassic magmatism in SW Tibet: petrogenesis and implications for India intra-continental subduction beneath southern Tibet. Lithos 113, 190–212.

Zindler, A., Hart, S., 1986. Chemical geodynamics. Annual Review of Earth Planetary Science Letters 14, 493–571.